Advances on methane reforming in solid oxide fuel cells

Fan, Liyuan; Li, Chao'en; van Biert, Lindert; Zhou, Shou Han; Tabish, Asif Nadeem; Mokhov, Anatoli; Aravind, Purushothaman Vellayani; Cai, Weiwei

DOI
10.1016/j.rser.2022.112646

Publication date
2022

Document Version
Final published version

Published in
Renewable and Sustainable Energy Reviews

Renewable and Sustainable Energy Reviews 166 (2022) 112646

Contents lists available at ScienceDirect

Renewable and Sustainable Energy Reviews

journal homepage: www.elsevier.com/locate/rser

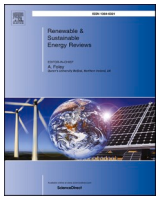

Advances on methane reforming in solid oxide fuel cells

Liyuan Fan [a,*], Chao'en Li [b], Lindert van Biert [c], Shou-Han Zhou [a], Asif Nadeem Tabish [d], Anatoli Mokhov [e], Purushothaman Vellayani Aravind [e], Weiwei Cai [f]

[a] College of Science and Engineering, James Cook University, 1 James Cook Drive, Townsville, QLD, 4811, Australia
[b] CSIRO Energy, 71 Normanby Road, Clayton North, Victoria, 3169, Australia
[c] Department of Maritime & Transport Technology, Delft University of Technology, Mekelweg 2, 2628, CD, Delft, the Netherlands
[d] Department of Chemical Engineering & Center for Energy Research and Development, UET Lahore (New Campus), 39021, Pakistan
[e] Energy and Sustainability Research Institute Groningen, University of Groningen, Groningen, 9700, AB, the Netherlands
[f] Sustainable Energy Laboratory, Faculty of Materials Science and Chemistry, China University of Geosciences Wuhan, Wuhan, 430074, China

ARTICLE INFO

Keywords:
Hydrogen production
Methane reforming kinetics
System modelling
Solid oxide fuel cells
Biogas

ABSTRACT

With the demand for anticipated green hydrogen and power production, novel and upgraded catalytic processes are desired for more effective utilization of precious natural resources. Methane steam reforming is an advanced and matured technology for converting methane to hydrogen and syngas. As a renewable energy resource containing a large amount of methane, biogas is a promising fuel for green hydrogen production. Because of the fuel flexibility and high efficiency relative to alternative technologies, solid oxide fuel cells with internal methane reforming capabilities may become an economically viable technology for hydrogen and power generation. A renewed interest in the flexible application of biogas in solid oxide fuel cells for the co-generation of green hydrogen and power has emerged recently, driven by the spectacular advances in fuel cell technology. However, the methane reforming process suffers from inaccurate or unprecise descriptions. Knowledge of the factors influencing the reforming reaction rate on the novel and improved reforming anode catalysts in solid oxide fuel cells are still required to design and operate such systems. Therefore, a comprehensive review of recent advances in methane steam reforming provides meaningful insight into technological progress. Herein, major descriptors of the methane steam reforming reaction engineering are reviewed to provide a practical perspective for the direct application of biogas in solid oxide fuel cells, which serves as an alternative sustainable, flexible process for green hydrogen and power co-production. Current advances and challenges are evaluated, and perspectives for future work are discussed.

1. Introduction

Climate change has become a major source of concern for the general public in recent years. Policies such as the Kyoto protocol [1] and the Paris agreement [2] have been put in place to limit the impact of global warming to a maximum temperature change of 2 °C above pre-industrial levels by reducing greenhouse gas (GHG) emissions. About 19% of the world's energy is currently supplied by non-fossil resources, such as biomass [3–5], biofuels, nuclear, solar photovoltaic, hydropower, geothermal, or wind energy. Fortunately, the supply of renewable energy resources has steadily increased thanks to the improved energy processing technologies and strict policies for greenhouse gas emissions [6–8]. Predictions indicate that by 2050, non-fossil fuels will make up 46% of the world's energy source.

Furthermore, there is a great concern about energy security because global oil production will not meet the demand within the next 10–20 years [6,9,10]. As a result, the application of renewable and sustainable alternative sources is under development to mitigate global energy and climate concerns. For example, many states in the USA have a long-term goal of achieving 100% renewable electricity-supported grids by 2050. In Australia, New South Wales (NSW) also has a long-term plan to achieve net-zero GHG emissions by 2050 [4,11]. However, the uptake of renewable energy is constrained by its stability and sustainability of supply, adequate distribution, and availability when required.

As a renewable energy carrier, hydrogen (H_2) has the potential to play a significant role in sustainable energy systems [12,13]. H_2 generated from biomass is considered green H_2 as the CO_2 released during the H_2 generation process is mainly compensated by the amount

* Corresponding author.
E-mail address: liyuan.fan@jcu.edu.au (L. Fan).

https://doi.org/10.1016/j.rser.2022.112646
Received 3 March 2022; Received in revised form 13 May 2022; Accepted 26 May 2022
Available online 3 June 2022

of CO_2 absorbed while biomass grows [5,14]. A study conducted by the European Fuel Cells and Hydrogen Joint Undertaking (FCH-JU) on green H_2 production has analyzed the possible pathways to produce H_2 from renewable energy sources. H_2 production via biomass gasification and biogas reforming is a promising method [15]. Furthermore, as biogas naturally contains a large amount of CH_4, it is a good fuel option for SOFCs where CH_4 can be internally reformed on the anode, thus making direct use of the heat and H_2O produced internally [16–20]. Integrating biomass processing technologies, such as gasification, gas cleaning, and upgrading processes, with SOFC technology, can provide more efficient design and simple operation conditions for power and H_2 production [5,21–24]. The direct electrochemical oxidation of CH_4 is substantially slower than that of H_2 and CO. CH_4 is assumed to be reformed to syngas before electrochemical oxidation. Direct internal reforming (DIR) of methane (CH_4) in SOFCs can achieve high electrical efficiencies and even higher efficiencies when applied for combined heat and power (CHP) [25–28], combined cooling, heating, and power (CCHP) [29–32] and combined heat, H_2, and power (CHHP) [7,33]. This review will not expand on these topics, and the interested readers can refer to the studies mentioned above for more details.

The SOFC is a fuel-flexible electrochemical device that can utilize various fuels to co-produce H_2 and power under proper operation conditions [34,35]. The typical lifetime of state-of-the-art stationary SOFCs is 40,000 h. A single SOFC consists of porous electrodes, a non-porous electrolyte, and interconnects. These can be repeated in a tubular or planar pattern to create a SOFC stack. A schematic illustration of the SOFC's working principle is shown in Fig. 1. The electrochemical reactions are relatively fast if the electrode materials are porous, electronically conductive, and catalytically active. Air/oxygen (O_2) is supplied to the cathode, where O_2 is reduced into oxide ions (O^{2-}) by gaining electrons at the triple phase boundary (TPB) on the cathode side in R1:

$$O_2 + 4e^- = 2O^{2-} \quad \text{(R1)}$$

The cathode must reduce O_2 and have sufficient conductivity to provide electrons for this reaction. The readers can refer to the review reported by Sun et al. [36] for more detailed information on the requirement and development of the cathode materials. O^{2-} then travels through the electrolyte towards the anode at the TPB, where they oxide the fuel, as shown in Fig. 1. In case H_2, the overall electrochemical oxidation reaction can be written as R2:

$$H_2 + O^{2-} \rightarrow H_2O + 2e^- \quad \text{(R2)}$$

SOFCs have been thoroughly researched throughout the literature for all ranges of parameters in experimental studies and computational investigations [22,37,38]. In principle, solid oxide fuel cells (SOFCs) can run on any fuel that can react with oxide ions coming through the electrolyte from the cathode to the anode. Therefore, it is regarded as one of the most promising candidates for alternative power generation technology, with high energy efficiency and flexibility as a power and H_2 co-producing device. While current SOFCs have demonstrated excellent performance when fuelled with various hydrocarbons, including biogas, significant challenges remain for practical applications [39]. For example, SOFCs produce power and heat by converting the chemical energy of the fuel through MSR, Water Gas Shift (WGS), and electrochemical (half) reactions. Coupling the endothermic reforming and exothermic electrochemical reaction in a single device may lead to local hot and cold spots, inducing unacceptable thermal stresses on the brittle ceramic materials [40]. In addition, several undesirable side reactions may form solid carbon deposits, blocking and damaging the porous electrodes [41]. However, an excessive supply of a reforming agent can suppress the formation of carbon or even remove it but might also oxidize the Ni catalyst in the fuel electrode [42]. Finally, it is difficult to optimize the catalyst for the different internal reactions simultaneously, compromising overall performance [43]. Therefore, a comprehensive understanding of the internal reforming process and its kinetics is indispensable.

Direct CH_4 oxidation in SOFCs is difficult to achieve electrochemically and is more likely to occur as a multi-step process. Therefore, Gur's in-depth review is recommended for a detailed discussion on the kinetics of direct CH_4 oxidation [21]. The effects of material, temperature, current, fuel composition, flow rate, and other experimental parameters on SOFC performance and efficiency have been extensively studied [44–51]. Since the potential utilization of renewable hydrocarbon fuels is a crucial advantage of SOFCs, studies of CH_4 reforming on the existing application of biogas in SOFCs for H_2 and power production in various simulations and experiments are very important for the development of such systems. Therefore, the CH_4 reforming in SOFCs and its applications for power and H_2 co-production is reviewed comprehensively in this review. The various CH_4 reforming kinetic models used in the modelling studies of such systems have been categorized and discussed in detail based on the deviation in complexity and reported assumptions of the models. In summary, this review provides an in-depth examination of the process of CH_4 reformation in SOFCs, providing insight into the potential of using CH_4 derived from a variety of sustainable sources to co-produce power and H_2 in SOFCs. Further research in this area is identified to accelerate the implementation of green H_2 production using biogas-fed SOFCs and provide significant benefits for climate change and energy security.

2. Modelling studies of methane reforming in SOFCs

CH_4 reforming chemistry is rich and includes various reactions, depending on the available agent, H_2O, O_2, and CO_2 or their mixture. Methane steam reforming (MSR) is the extensively utilised and well-developed of these reforming processes because steam reforming of

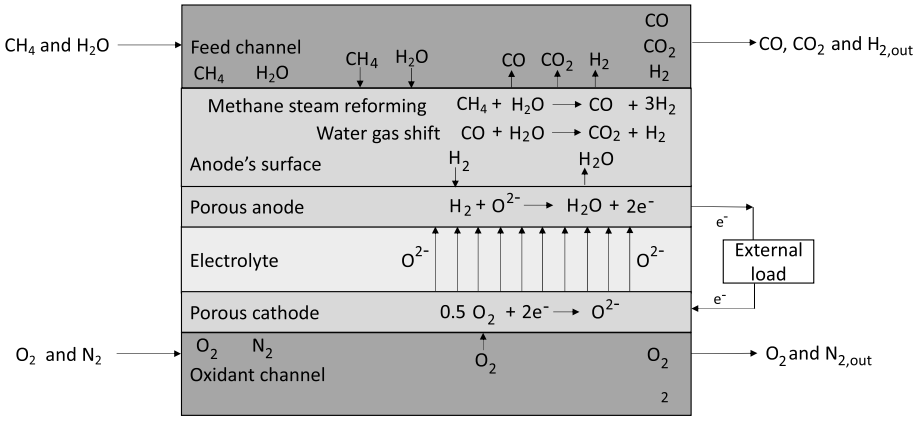

Fig. 1. The methane steam reforming and electrochemical reactions on SOFC anode.

natural gas in centralized plants produces approximately 75% of the H_2 produced globally [16]. As shown in Fig. 1, MSR is a catalytic process expressed in R3 (H_{298} = +206 kJ/mol) [52]:

$$CH_4 + H_2O \rightarrow CO + 3H_2 \quad \text{(R3)}$$

The CO, besides electrochemical oxidation, is also converted to CO_2 through R4, the water-gas shift (WGS) reaction (ΔH_{298} = −41 kJ/mol) [53], thus maximizing the production of H_2:

$$CO + H_2O \leftrightarrow CO_2 + H_2 \quad \text{(R4)}$$

In dry methane reforming (DMR), CO_2 is used as an oxidant in place of H_2O (ΔH_{298} = +247 kJ/mol) shown in R5 [54]:

$$CH_4 + CO_2 \rightarrow 2CO + 2H_2 \quad \text{(R5)}$$

Interest in this technique is mainly driven by the possibility of capturing and reusing both CH_4 and CO_2. However, besides the high energy duty, another critical issue is the requirement for a nearly pure source of CO_2 as feedstock.

Partial oxidation of Methane (POM) is an exothermal reaction (ΔH_{298} = −38 kJ/mol), which proceeds in R6 [39]:

$$CH_4 + \frac{1}{2}O_2 \rightarrow CO + 2H_2 \quad \text{(R6)}$$

Auto thermal reforming is a hybrid process combining POM with conventional MSR. As the process does not require an external heat source, auto thermal reforming can increase the thermal conversion efficiency of H_2 production and reduce its operational costs. Depending on the purity requirement of the application, syngas production is usually followed by a further purification step. The latter can be achieved using conventional (pressure swing adsorption and cryogenic distillation) or unconventional (membrane separation) technologies [55].

SOFCs are the most promising fuel cell type for CH_4 reforming, opening new avenues for developing green, energy-efficient, and cost-effective H_2 and power co-production technology. One advantage is the fuel flexibility. Since the early 2000s, researchers have been studying the operation of SOFCs on a variety of sustainable fuels, including natural gas, biogas, syngas generated from biomass gasification, and distillate fuel reforming [10,35,42,56–59]. Using different hydrocarbon fuels directly would lower fuel prices and accelerate SOFC adoption, especially for high-value applications [37,39,60–62].

However, fuelling SOFCs with hydrocarbon fuels is inherently complex due to physiochemical, thermal, and transport processes. Given the possibility of competing or co-existing multiple reforming reactions at the SOFC anode, studying the mechanism of CH_4 reforming at SOFC operating conditions is a logical first step toward achieving direct CH_4 application. Thus, modelling studies are advantageous for forecasting the operating safety restrictions and designing SOFCs suited for various fuels before actual testing [63–66]. The equilibrium is valuable for anticipating the safety of cells and stacks and the possibility of fuelling them with practical fuels which contain contaminants such as HCl and H_2S [67,68]. System-level modelling can generate the data necessary to develop a holistic view of the system, thus studying its operational regimes, including safety, reliability, and performance [26,57]. The computational fluid dynamic (CFD) simulation is another tool to examine the distribution of mechanical, chemical, and thermal parameters within the system that helps in optimizing the component and system designs [69,70].

There are multiple commercial tools to simulate the SOFC operations, including Aspen Hysys® (Aspen Tech), Aspen Plus® (Aspen Tech), ChemCAD® (Chemstations), COCO/COFE® (AmsterCHEM), CycleTempo (Asimptote), DWSIM® (Open Source CAPE-OPEN process simulator), gPROMS® (Siemens Process Systems Engineering), ProSimPlus (ProSim), SimSci PRO/II® (SimSci/Invensys), UniSim® (Honeywell), Comsol ®, and Ansys ®. These software packages can calculate the material and energy balances, the equipment size, and the cost of several chemical processes, including fermentation, distillation, combustion, gasification, separation, filtration (microfiltration, ultrafiltration, and reverse osmosis), chemical extraction, absorption, adsorption and crystallization. They can also increase productivity and solve chemical process models, modelling, evaluating, and optimizing SOFC systems in a user-friendly environment [63]. These programs have been used for simulations with kinetics implemented in zero-dimensional (0D), one–dimensional (1D), and two–dimensional (2D) models to identify profiles of gas concentration, voltage (V), and feed utilization throughout the SOFC anode [71]. However, models using such software need an accurate description of the reforming process of CH_4.

Yi et al. [72] developed a theoretical framework and thermodynamic simulation capability to investigate an integrated SOFC reformer system working on multiple fuels. The results indicated that feeding various fuels in the same system may present major thermal management issues. Proper operation on different fuels may require significant modifications in operating conditions or system design.

Audasso et al. [73] performed 2D simulations of the direct internal reforming process to study performance degradation and optimize SOFC operating conditions. The developed model may simulate overall cell performance and evaluate the local variables that provide theoretical and feasibility studies insights. Moreover, the model is computationally lean and can be integrated into more complex software for system/plant simulations, such as Aspen Plus.

Another 2D model is developed by Xu et al. [74] to address the carbon deposition problem in SOFCs. The electrolyte can help prevent carbon build-up and lower cell performance by transporting O_2 molecules to the fuel side from the cathode. After being validated by experimental data, the model is expanded to a tubular cell for parametric simulations. All porous SOFCs' carbon resistance and electrochemical performance are investigated under various operating conditions with electrolyte microstructure features. All porous SOFCs have good carbon resistance, as shown quantitatively. The fuel composition and flow rate influence the anode surface's electrochemical performance and oxygen-to-carbon ratio. The findings of this study provide a strong foundation for understanding the principles of operation and promising premises of SOFCs operating with hydrocarbon fuels.

A SOFC stack model comprising 100 anode-supported cells cogenerator with biogas was presented by van Herle et al. [75]. A process flow diagram was defined to vary system operation parameters, including fuel composition, reforming process, stack temperature, current, and fuel utilization. This model can also predict the performance of complex fuel sources such as sewage, landfill sites, and large farms. However, the absence of reforming kinetics and electrode diffusion overpotentials are the shortcomings of this model.

SOFC models for the individual cell or stack are developed using a CFD environment, which may forecast cell potential and the spatial distribution of current density, chemical concentrations, and temperature as time functions for various cell geometries and operating conditions [47,77]. CFD models can also evaluate the effects of different operating variables on SOFC performance. Fan et al. [76] investigated the fuel flexibility of an anode-supported intermediate temperature planar SOFC under co-flow operation using a single channel model containing direct internal reforming (DIR). In Fig. 2, the three reactions considered in this modelling work are the MSR, the WGS, and the electrochemical oxidation of H_2. For the safe operation of biogas-fuelled SOFCs, thermodynamic calculations of Ni oxidation and carbon deposition were performed. The SOFC anodes can be protected against carbon deposition by incorporating enough reforming agents into the fuel stream. While kinetics of carbon deposition and reoxidation is vital in utilizing hydrocarbon fuels, a good understanding of CH_4 reforming kinetics is the first necessary step. It will benefit in overcoming the operational safety and stability issues. When fuelling a SOFC with CH_4, the reforming kinetics will significantly affect gas and temperature distributions. These parameters largely determine the fuel cell system performance and occurrence of carbon deposition and thermal stresses

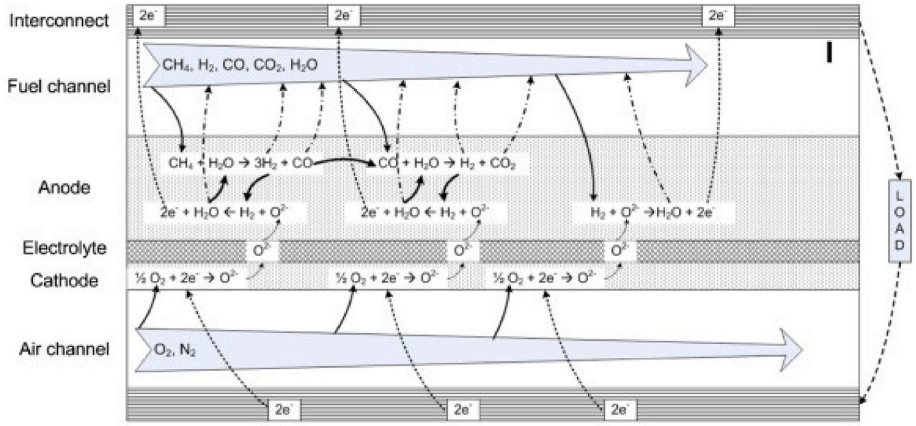

Fig. 2. Schematic representation of reaction and transport processes in the SOFC (Reprinted with the permission from Ref. [76], Copyright (2013), Elsevier).

[44,63]. Because different reforming kinetics have been published in the literature and using them in SOFC simulation may produce varied results. A comparative analysis is required to examine the impact of such kinetic factors on cell performance. The experimental literature on MSR kinetics is thoroughly reviewed and carefully incorporated into this model to determine how internal MSR processes affect cell performance [45,64,78–82]. Based on different reforming kinetics, the modelling results reveal differences in the operational parameters such as current density, temperature, and gas concentration. Calculations of the internal reforming reaction and the possibility of undesirable side reactions are provided, along with recommendations for future theoretical and experimental investigation.

Using the most generally used rate expression described by Achenbach and Riensche [83] was also conducted by Fan et al. [76,77]. However, the Ni concentration (20 wt%) was lower than the 50–70 wt% typically seen in SOFC anodes. In addition, the experimental data collected in this study cannot be directly applicable to other research because of the incompatible operating parameters, such as the anode thickness and feed gas compositions. Another rate expression reported by Xu and Froment [84] was used by Lehnert et al. [85], where first-order dependences of CH_4 and H_2O concentrations were assumed. However, the latter is rarely observed in laboratory experiments, especially under conditions relevant to direct internal MSR in SOFCs. Therefore, reliable CH_4 reforming kinetic models are needed to describe the reforming process in SOFCs accurately.

Heterogeneous catalysis for MSR over SOFC anode materials must consider the catalyzed reaction and the complexity of the SOFC anode microstructure, contamination of catalytic sites, and adsorption and desorption kinetics. Most research on the MSR reaction kinetics has been conducted during the last decades, particularly on Ni-based catalysts. A considerable variation of MSR kinetics derived from the experimental data was obtained under different testing conditions, including (1) different catalysts; (2) different Ni content/catalytic loadings; (3) various conditions like temperature, steam to carbon ratios, the interaction of electrochemical reactions with the reforming reaction; and (4) different proposed kinetic models and mechanisms. Consequently, there is no single universal model applied in every MSR kinetic study, and the majority of existing data is interpreted through various types of kinetic models. In these SOFC kinetic studies, three types of MSR kinetic models can be distinguished: the multi-step reaction mechanism [78,79,84,86,87], the surface reaction model assuming a rate-determination step on the surface of a catalyst, and the empirical global gas-phase rate expression [45,78,79,81,83,88–96]. The proposed rate expressions vary among various kinetic models, including First-Order (FO), Power-Law (PL), Langmuir–Hinshelwood (LH), and Langmuir–Hinshelwood–Hougen–Watson (LH-HW). These are categorized based on the practicality of applying modelling studies to accurately describe the reforming process and reviewed in the following subsections.

3. Methane steam reforming kinetic models

3.1. Multi-step reaction mechanism

Heterogeneous catalysis is a multistep reaction that involves a sequence of elementary reaction steps [97]. Kinetic studies for MSR were given particular regard, and various kinetic parameters for MSR were reported. Kinetic models can be derived from experimental data, yielding characteristic parameters that describe a reaction. Hecht et al. [98] and Zhu et al. [93] have developed a multistep reaction mechanism for CH_4 reforming on Ni-based SOFC anode. The mechanism comprises 42 reactions involving six gas-phase species and twelve surface adsorbed species. The mechanism encompasses heterogeneous reforming, WGS, and Bouduard reactions [84]. They have also reported a computational model for heterogeneous chemistry and electrochemistry in SOFCs over Ni-based anode materials using the proposed multi-step elementary reactions. A multicomponent transport model based on kinetic theory is used to describe the transport of a gas mixture through a porous matrix of evenly distributed particles. Charge-transfer chemistry is described using a modified Butler-Volmer equation derived from elementary reactions and assuming a single rate-limiting charge transfer process. The underlying theory, on the other hand, is unaffected by geometry. The representation of elementary heterogeneous kinetics in multi-step reaction mechanisms is a key new model feature in SOFCs fed with CH_4-containing fuels. The model considers the effects of channel flow, porous electrode transport, heterogeneous-reforming processes, partial-oxidation chemistry, and electrochemistry. Analyzing oxidative MSR on Ni catalysts helped confirm the heterogeneous chemical reaction process.

Following the investigations by Hetch et al. [98], Janardhanan et al. [99] modelled the internal CH_4 reforming SOFC performance coupled with interactions of transport, heterogeneous catalysis, and electrochemical processes. Experimental data and anticipated cell performance are found in good agreement. At the TPB, the H_2O content significantly impacts the overpotentials and the coverage of surface species. Understanding the underlying chemical processes and optimizing physical operations in any fuel cell can be accomplished using this model.

Wei et al. [96] assessed the reaction mechanisms of CH_4 with CO_2 or H_2O to form syngas and carbon on Nickel–Magnesium Oxide (Ni–MgO) catalysts. The sequence of elementary steps shown in Fig. 3 accounting for CO_2 or H_2O reforming, reforming, CH_4 decomposition, and WGS reactions also provide the steps required to form chemisorbed carbon precursors to carbon filaments. All of the general characteristics of this sequence are in complete agreement with the previously hypothesised

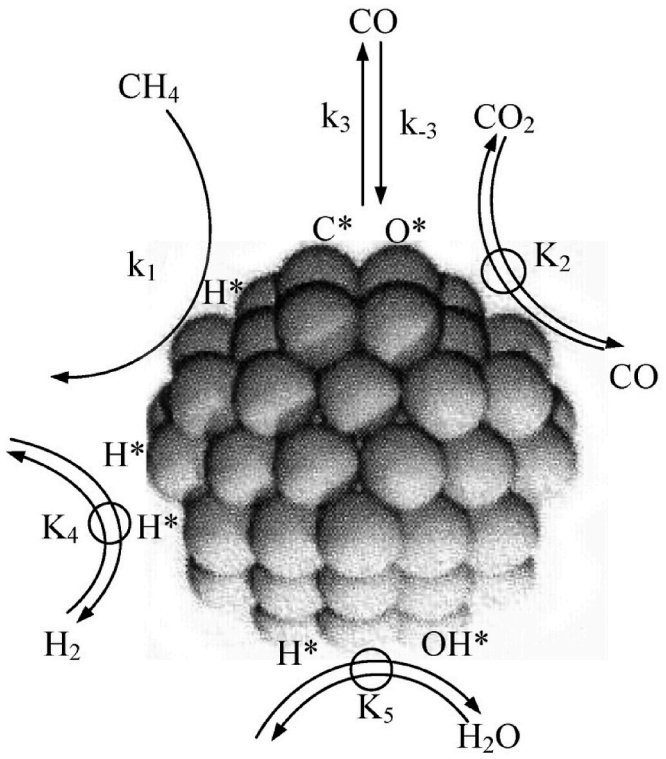

Fig. 3. The sequence of elementary steps for CH_4-reforming and water– gas-shift reactions on Ni-based catalysts (fx1irreversible step, fx1quasi-equilibrated step, fx1 reversible step, k_i is the rate coefficient, and K_i is the equilibrium constant for a given step i) (Reprinted with the permission from Ref. [96], Copyright (2004), Elsevier).

mechanism by Bebelis et al. [92] on supported Ni catalyst. Reaction rates, rate constants and kinetic parameters for the forward CH_4 reactions were identical, indicating that the C–H bond activation is the only kinetically relevant step and reversible. The proposed elementary processes provide a good framework for dealing with the dynamics of carbon synthesis during CH_4 reforming, as evidenced by kinetic and isotopic evidence. The partial pressure ratios of various species in the contacting gas phase are linearly connected to the rate of carbon production and thermodynamic activity of chemisorbed species.

Jones et al. [100] performed first-principles calculations and experiments on CH_4 reforming over transition metal catalysts. The authors presented a detailed analysis of the reforming process based on experimental observations and proposed nine elementary reactions to represent the MSR reaction. The study considers the adsorption during the reforming process on transition metal surfaces and a series of elementary steps for the MSR reaction. It demonstrates that by integrating scaling principles with thermodynamics and kinetics, one can estimate the catalytic activity of pure metals. A CH_4 dissociation step and a CO formation step are kinetically controlled by the reaction, with the last step dominating at lower temperatures. In a catalyst, CH_4 reforming is a multi-step chemical process that includes gas phase and surface reactions and is highly dependent on operating conditions. The rates of elementary steps are either known with a limited accuracy or are uncertain. As a result, calculating the MSR reaction rate from the rates of elementary steps remains challenging.

3.2. Surface reaction model

Multi-step reaction mechanisms may be reduced to a surface reaction model when a single step is assumed to be rate-determining.

The commonly used LH model shown in Fig. 4(a) represents a catalyst-based mechanism wherein participating species chemisorb onto a heterogeneous catalyst surface in a monolayer and react while adsorbed [79], reflecting the first two scenarios. The Hougen-Watson theory is required to find the rate-controlling step and realize the entire reaction process. The underlying assumption is that a reactant is adsorbed onto the catalyst's surface and subsequently reacts to form the product. The theory is based on the following assumptions: (1) adsorption occurs exclusively on a solid surface's top monolayer; (2) the energy distribution on the surface is uniform; and (3) the adsorbed species do not react with one another.

The surface reaction can be either a single site or dual-site. The site where the reactant is adsorbed in a single-site mechanism participates in the reaction. For example, assuming dissociative adsorption of CH_4 and H_2O on a singular or identical site [101], as shown in R7-18:

$$CH_4 + 2X \leftrightarrow CH_3 - X + H - X \quad (R7)$$

$$CH_3 - X + X \leftrightarrow CH_2 - X + H - X \quad (R8)$$

$$CH_2 - X + X \leftrightarrow CH - X + H - X \quad (R9)$$

$$H_2O + 2X \leftrightarrow OH - X + H - X \quad (R10)$$

$$OH - X + X \leftrightarrow O - X + H - X \quad (R11)$$

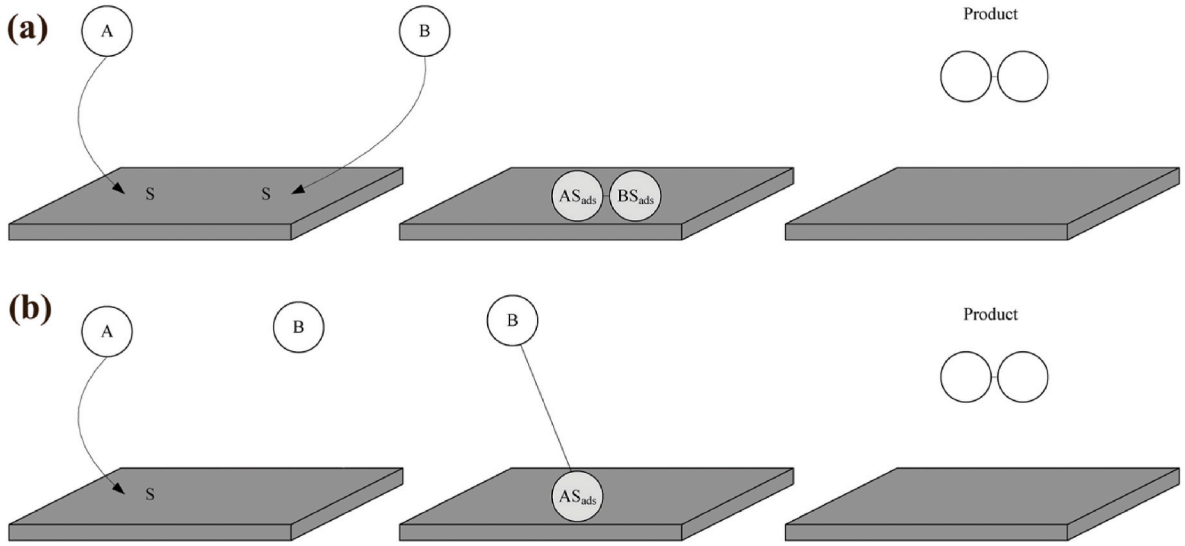

Fig. 4. (a) Langmuir-Hinshelwood kinetic model diagram; (b) Eley–Rideal kinetic model diagram.

$$CH - X + O - X \leftrightarrow CHO - X + H - X \quad (R12)$$

$$CHO - X + X \leftrightarrow CO - X + H - X \quad (R13)$$

$$CHO - X + O - X \leftrightarrow CO_2 - X + H - X \quad (R14)$$

$$CO - X \leftrightarrow CO + X \quad (R15)$$

$$CO_2 - X \leftrightarrow CO_2 + X \quad (R16)$$

$$2H - X \leftrightarrow H_2 - X + X \quad (R17)$$

$$H_2 - X \leftrightarrow H_2 + X \quad (R18)$$

Or assuming preferential dissociative CH_4 and H_2O adsorption on two active sites X_1 and X_2 [101], called a "double-site mechanism", as shown in R19-31:

$$CH_4 + 2X_1 \leftrightarrow CH_3 - X_1 + H - X_1 \quad (R19)$$

$$CH_3 - X_1 + X_1 \leftrightarrow CH_2 - X_1 + H - X_1 \quad (R20)$$

$$H_2O + 2X_2 \leftrightarrow OH - X_2 + H - X_2 \quad (R21)$$

$$OH - X_2 + X_1 \leftrightarrow O - X_1 + H - X_2 \quad (R22)$$

$$CH_2 - X_1 + O - X_1 \leftrightarrow CHO - X_1 + H - X_1 \quad (R23)$$

$$CHO - X_1 + X_1 \leftrightarrow CO - X_1 + H - X_1 \quad (R24)$$

$$CHO - X_1 + O - X_1 \leftrightarrow CO_2 - X_1 + H - X_1 \quad (R25)$$

$$CO - X_1 \leftrightarrow CO + X_1 \quad (R26)$$

$$CO_2 - X_1 \leftrightarrow CO_2 + X_1 \quad (R27)$$

$$2H - X_1 \leftrightarrow H_2 - X_1 + X_1 \quad (R28)$$

$$2H - X_2 \leftrightarrow H_2 - X_2 + X_2 \quad (R29)$$

$$H_2 - X_1 \leftrightarrow H_2 + X_1 \quad (R30)$$

$$H_2 - X_2 \leftrightarrow H_2 + X_2 \quad (R31)$$

A reaction between an adsorbed molecule and a gas phase molecule serves as a third mechanism. The Eley–Rideal (ER) mechanism explains a reaction between a chemisorbed reactant and another non-chemisorbed reactant, as shown in Fig. 4(b). Single-layer adsorption, no diffusion limit, and only the reactants affect the reaction rate are some of the approximations. Hofmann et al. [102] analyzed the heterogeneous reaction mechanism published by Hecht et al. [98] into a simplified model. The CH_4 reforming is represented using a global kinetic approach, and the WGS reaction is assumed to be in equilibrium. The catalytic surface coverage can be calculated using the model.

Individual steps for the adsorption or desorption of various species during CH_4 reforming on different Ni surfaces were investigated experimentally and numerically by Delgado et al. [103]. The main pathways for CH_4 conversion processes on the Ni catalyst for H_2 and CO productions are shown in Fig. 5. A model consisting of 52 reactions with six gas-phase species and 14 surface species involving adsorption and desorption steps of all reactants, products and surface reaction steps was proposed. The availability of adsorbed atomic oxygen O(s), produced via dissociative adsorption of oxygen-containing species, plays a vital role in determining the reaction rates supported by the DFT studies [104–107]. A detailed reaction mechanism for CH_4 reforming was developed and evaluated, making it possible to predict the product distribution for methane conversion in the reactor. The developed simulation tools simulate the chemical species profiles and the surface coverage within the reactor.

The heterogeneous reactions have multiple elementary steps that compete with one another. According to this theory, any of the three groups can determine the reaction rate: (1) kinetic group, (2) driving force group, and (3) adsorption group [97]. For a hetero-catalytic reaction, a general form of rate expression could be expressed in Eq (1):

$$r = \frac{(kinetic\ factor)\cdot(driving\ force)}{(adsorption\ isotherm)} \quad (1)$$

In the MSR reaction, assuming a single layer surface hetero-catalytic reaction, the general adsorption isotherm is calculated in Eq (2):

$$adsorption\,isotherm = \left(S_0 + K_{CO}p_{CO} + K_{H_2}p_{H_2} + K_{CH_4}p_{CH_4} + K_{H_2O}p_{H_2O}\right)^n \quad (2)$$

Each term is proportional to the surface coverage by the respective species, scaled such that S_0 is proportional to the vacant surface. n is the

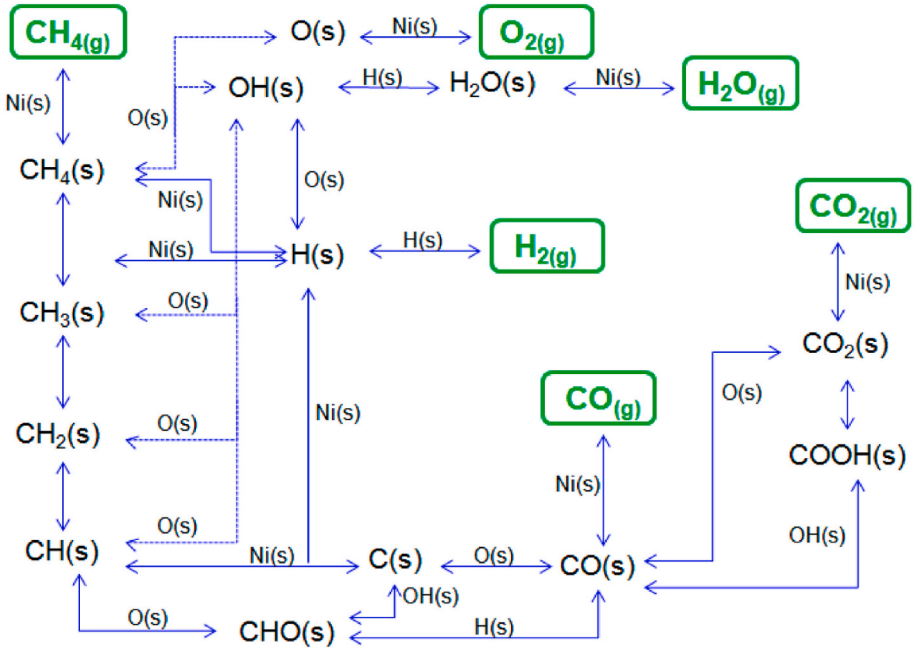

Fig. 5. Reaction pathways for methane oxidation and reforming on the nickel-based catalyst (Reprinted with the permission from Ref. [103], Copyright (2015), MDPI).

number of sites involved in the molecular reaction. The assumption of the bimolecular rate-determining step as the kinetic term can be combined with the Langmuir isotherms to describe the adsorption to the catalyst surface. The temperature dependence of the adsorption coefficient K_j typically follows the van't Hoff equation. The driving force of the reaction is calculated based on the deviation from reaction equilibrium. It can be calculated via the reaction quotient and a temperature-dependent equilibrium constant, where the reaction quotient has been expanded to the MSR reaction. The driving force is calculated in Eq (3) [108]:

$$driving\ force = 1 - \frac{p_{CO} \cdot p_{H_2}^3}{K_{eq,wgs} \cdot p_{CH_4} \cdot p_{H_2O}} \tag{3}$$

The equilibrium constant for the WGS reaction ($K_{eq,wgs}$) is a function of temperature, calculated using empirical equations [84].

The general kinetic factor is calculated in Eq (4):

$$kinetic\ factor = k \cdot p_{CH_4}^a \cdot p_{H_2O}^b \cdot p_{H_2}^c \cdot p_{CO}^d \tag{4}$$

Experiments were carried out to evaluate the performance of MSR activity over a Nickel–Magnesium Aluminate (Ni–$MgAl_2O_4$) catalyst, and an effective kinetic model was developed based on the kinetic model proposed by Xu and Froment [84], in which an intrinsic expression for the reforming reaction rate was proposed. The model has been widely accepted as a reliable approximation of MSR kinetics. However, compared to commercial SOFC anodes, which typically have Ni contents ranging from 50 to 70 wt %, this one had a lower Ni concentration (20 wt%). Lehnert et al. [85] applied the MSR kinetic parameters obtained by Xu and Froment [84] to an industrial catalyst. Elnashaie et al. [109] employed the LH reforming rate expression to assess the impact of non-monotonic kinetics on the performance of steam reformers, which explains the discrepancies between the rate expressions found in the literature. Experiments were also carried out by Hou et al. [87] to study the kinetics of the MSR over a commercial Nickel-αAluminum Oxide (Ni-αAl_2O_3) catalyst. The reforming reaction rate increases in proportion to the CH_4 partial pressure at low product concentrations. The surface reaction between adsorbed species was identified as the rate-controlling step. The intrinsic rate expressions were obtained using the LH-HW method and Freundlich's adsorption theory. The simulation determined a satisfactory model of intrinsic kinetics. Klein et al. [110] modelled the direct internal and gradual internal reforming SOFCs using the kinetic parameters reported by Hou et al. [87]. The kinetic data were obtained from testing a Ni-αAl_2O_3 catalyst, different from the commonly used anode materials.

Dicks et al. [86] studied the MSR reaction on Nickel-Yttria-Stabilized Zirconia (Ni-YSZ) in a tubular plug flow differential reactor. They developed an improved MSR rate expression assuming LH adsorption isotherms. The reaction showed first-order dependence on CH_4, weak positive dependence on H_2, and strong negative dependence on H_2O. Because reaction orders in H_2 and H_2O were allowed to vary for different temperatures and gas compositions, the kinetics were convoluted.

Bebelis et al. [92] investigated the MSR catalytic activity and kinetics of a Ni-YSZ anode. The reaction followed an LH kinetic pattern, indicating that CH_4 and H_2O adsorption on the catalytic sites was competitive. The apparent activation energy is greatly influenced by two rate-determining steps: the activated adsorption of CH_4 for the formation of active species and the surface reaction between the adsorbed activated carbon and O_2 for the production of CO.

Additional factors need to be considered due to the complicated nature of the adsorption-desorption mechanism. Different anode manufacturing processes result in varying catalyst availabilities for the adsorbed species. Combined with diffusion and heat/mass transfer limitations, this can result in deviations from the actual results. These problems may have a more significant impact on reforming behaviour than the kinetics of the surface reaction itself. To combat this issue, Wang et al. [111] implemented an 'effective factor' that can be experimentally calculated and acts as a rate coefficient, allowing greater model adherence to the physical behaviour, although at the cost of computing time. Furthermore, the need for additional kinetic parameters is still not thoroughly demonstrated in the literature.

Thallam Thattai et al. [79] emphasised the need for simply applicable global kinetic models for SOFC systems and a lack of research on MSR global and elementary kinetic mechanisms. They observed the limitations in using previously proposed rate expressions for Ni-based catalyst beds to analyse MSR kinetics of SOFC cermet anodes. Many PL and LH kinetic models for MSR on Ni-GDC anodes were developed and predict significantly different local MSR reaction rates and distributions of species concentrations, highlighting the need for further investigation. The following subsection examines a practical and balanced kinetic treatment based on simplifications and approximations.

3.3. Gas-phase reaction model

The PL kinetic model is the most simplified and commonly used reaction rate expression in modelling studies. This model simplifies the reforming reaction kinetics by assuming a global singular reaction step for a given reaction, determined via a set of experimentally determined variables. A fundamental principle of this model is that the rate of every chemical reaction is proportional to the masses of the reacting substances, as shown in Eq (5):

$$r = k \cdot p_{CH_4}^a \cdot p_{H_2O}^b \tag{5}$$

where p_{CH_4} and p_{H_2O} are the partial pressures of CH_4 and H_2O, and a and b are the reaction orders of CH_4 and H_2O, respectively. According to the previously published data, a typical range for these reaction orders is −2.0 to 2.0, according to the previously published data [44]. Reaction orders commonly resemble first-order for p_{CH_4}, and zero-order for p_{H_2O}.

Achenbach and Riensche [83] report a PL rate expression that has been extensively used in SOFC modelling studies. Ahmed and Foger [91] studied the MSR catalytic activity of basic Ni-YSZ and modified anode materials. A lower H_2O to CH_4 ratio was required to avoid carbon deposition. They used a PL kinetic model, and the orders for CH_4 and H_2O were higher on the modified anode. In addition, the activation energy was greater on the modified anode, showing that the active catalytic sites in these two anodes were distinct.

MSR on Ni–MgO catalysts at low pressure was investigated by Wei et al. [96]. A PL rate expression was used in this study with a lower temperature range. The reaction rate was proportional to p_{CH_4}, and independent of p_{H_2O}. In this study, a comparison of the reactivity of Ni and noble metal catalysts for CH_4 reforming was made using direct measurements of C–H bond activation rates. The activation energy was similar to that of the CH_4 decomposition, indicating the activation of the C–H bond is the rate-limiting step.

Experimental study of reforming kinetics and the influence of operation conditions on it are essential for an accurate prediction of the performance of a direct internal reforming SOFC. Internal reforming kinetic parameters have been reported by Mogensen et al. [90] on a complete cell with a Ni-YSZ anode under closed-circuit operations. The rate expression was proposed in a PL type with an activation energy of 166.1 kJ/mol. The reaction rate has a dependency on only p_{CH_4}, with a reaction order of 0.7. MSR over a Ni-YSZ anode in stack configuration was also studied by Mogensen et al. [82]. It was discovered that the rates could be well matched to a PL rate expression when the measurements were carried out between 600 °C and 800 °C under different pressures. According to the model, the CH_4 conversion in a stack configuration could be predicted from the inherent dynamics of the anode support materials, and the predictions were consistent with the experimental results in most cases. Because of its simplicity, this model is well suited for simple SOFC stack models, such as those used for flow sheeting applications such as Aspen Plus®.

Sciazko et al. [94] presented a novel approach to the experimental investigation of MSR kinetics utilizing the orthogonal least-squares method. The results were obtained using a plug flow tubular reactor with fine Ni-YSZ catalyst particles as a catalyst. The suggested algorithm is easily adaptable to mathematical modelling of the fuel reforming process on various catalysts and under different experimental conditions. Furthermore, the difference between the published inconsistent data about the reaction kinetic parameters can be clarified using this approach. Fan et al. [44,45] investigated MSR reaction kinetics in complete SOFC with Ni-YSZ and Ni-GDC anodes using this method under varying operating conditions. A PL rate expression was used in both studies. The CH_4 conversion reduces as the temperature decreases, consistent with earlier research. However, the MSR reaction rate increases slightly when a current is drawn. The effect of H_2O concentration on the reaction rate becomes more negative, likely due to the adsorbed O_2/H_2O molecules/ions blocking reaction sites or the local oxidation of Ni. Thallam Thattai et al. [79] extended the study and reported the modelling results of both PL and LH kinetic models derived from their previous experimental studies [45,78,79]. Both models have successfully predicted the spatial distribution of the reforming reaction.

PL type rate expression requires experimentally determined values of the pre-exponential factor, the activation energy, and the reaction orders to predict the reaction rates for given conditions. These parameters can be readily applied to systems with variant temperatures and inlet gaseous compositions when these parameters are obtained. Several studies, such as those conducted by Achenbach et al. [83] and Belyaev et al. [112] have assumed FO kinetics. This low-order model prioritized the computational time, which was reduced significantly through the first-order assumption, allowing for the development of a real-time feedback control system. However, this simplification sometimes is contrary to multiple experimentally produced data sources, showing reaction orders for CH_4 and H_2O vary across numerous experimental conditions.

3.4. Summary and comparison of methane steam reforming kinetic models

MSR kinetics on SOFC anodes have been widely studied. A large variety of reaction rate expressions has been proposed in different studies. The various reaction rate expressions may be selected and used in different modelling studies based on the anode materials and operation conditions. The previously reported PL and LH kinetics for MSR on Ni-based materials are summarized in Table 1. The WGS kinetic models over various catalysts are summarized in Table 2.

A vast majority of these studies used Ni-YSZ cermets. Kinetic data have also been reported on Ni-GDC anode materials. For the MSR kinetic studies, some researchers used Ni-based catalysts, such as Ni–$MgAl_2O_4$ cermet [91] and Ni-αAl_2O_3 catalyst [135], for the MSR kinetic studies. As reactions occur on the anode, which is perhaps the most critical factor for the operational performance of SOFCs. SOFC anode materials should ideally be chemically stable, have sufficient mechanical strength, and possess high conductivity and electro-catalytic activity. A series of MSR catalysts with increased activity and stability have been developed. They can be employed as anode catalysts in the SOFC, allowing for relatively inexpensive, safe, and readily available fuel cell development [37,46,128]. Many detailed, comprehensive overviews of those materials can be found in other reviews [128–135].

The reported values for the reforming activation energy differ from as little as 18 kJ/mol up to 240 kJ/mol [44,45,79,113]. Ni contents typically range from 50 to 70 wt%, close to the typical Ni content in SOFC anode materials. Few studies have reported the MSR kinetic parameters on materials with low Ni content [87,96,112,119]. Lee et al. [116] and Minette. et al. [81] reported MSR kinetics on high Ni content materials with a significant activation energy difference. Based on the catalyst materials used, these experimental studies can be broadly grouped into two categories: (1) Ni-based catalytic materials such as catalyst pellets [83,84,86,92,100,116,136]; (2) active SOFC anodes, such as the porous catalyst layer on the electrolyte support, under conditions with or without producing a current [44,45,78,79,90,91,113,137–140].

The experimentally derived reforming kinetics mainly were obtained within the same temperature range as the SOFC operating temperature, from 700 °C to 900 °C as shown in Table 1. Few studies have reported the reforming kinetic parameters below 600 °C. Xu et al. [84] have studied the reforming kinetics from 400 °C to 800 °C, and Hou et al. [87] have tested the catalytic activity from 450 °C to 550 °C. Most research was carried out on Ni-based catalytic materials operated within a safe range of steam to carbon ratios. The trials carried out in these studies were designed to avoid the formation of carbon deposits. With the elimination of carbon deposition during the reforming reaction, it may be possible to understand better how different operating conditions affect the reforming kinetics in SOFCs.

The overall reaction order in the PL kinetic model also varies significantly from 0.25 to 0.8. The LH exponents mainly were found to be 2. These variations in the reaction orders may be due to the various test materials, different steam to carbon ratios, and temperatures. Even with a similar Ni content in the anode materials, dopants and modifications can significantly impact the kinetic activity [79,95,113]. Mogensen et al. [82,90,141] investigated the kinetics of the internal MSR reaction on Ni-YSZ within a SOFC stack and externally via crushed Ni-YSZ pellets using a packed bed reactor. An expression for the rate of H_2 generation was derived via the PL kinetic model. The reaction orders were fixed to 0.9, −0.2, and 0.2 for CH_4, H_2, and CO_2, respectively. The activation energy was 185 kJ/mol. However, it was noted that this model on the packed bed had a mean absolute deviation of 43.7%.

Six CH_4 reforming reaction rates: four PL-type rate expressions and two LH-type rate expressions derived on different functional Ni-YSZ anodes versus temperature, the p_{CH_4} and p_{H_2O} are selected for the comparison, and the discussions are as follows.

The influence of temperature on the MSR reaction rates, converted to the standard surface reaction rate over Ni-YSZ anodes, was plotted in Fig. 6. The calculated reaction rates using the selected kinetic parameters increase exponentially along with temperature; however, they vary significantly given the same partial pressures of different species and temperatures. The variations may result from the material properties, such as the surface area, the microstructure of the anode materials, and operational conditions such as the temperature, the flow rate, and the steam to carbon ratio, indicating the challenge of developing a universal reforming rate expression.

The influence of p_{CH_4} on the MSR reaction rate over Ni-YSZ anodes is plotted and shown in Fig. 7 (a). Most of the calculated reaction rates increase linearly with CH_4 because most reaction orders for CH_4 are either one or very close to one. The influence of p_{H_2O} on the MSR reaction rate over various Ni-YSZ anodes were plotted and shown in Fig. 7 (b). Most of the calculated reaction rates slightly decrease with p_{H_2O} because many reaction orders for H_2O are very close to zero or slightly negative. However, the absolute reaction rates predicted by the previously reported kinetic parameters vary significantly for similar temperatures, flow rates, and species partial pressures. There are numerous reasons for these variations. The surface area of the anode materials, for example, and the microstructure of the anode materials are all affected by material properties, as are the temperature and steam to carbon ratio. This indicates the need for a more consistent reforming reaction rate expression.

4. Application of biogas in SOFCs

SOFC is a promising alternative technology that can convert CH_4 to power with potentially high efficiency. In addition, CO_2 can be separated relatively easily from the flue gas as air and fuel are not mixed in the SOFC. Therefore, biogas is a promising fuel for SOFCs. The CH_4 content typically ranges from 45 mol% to 75 mol%, most of the

Table 1
MSR kinetics of Ni-based materials.

Ref	Anode Material	Rate Expression	T (K)	Wt% Ni	SC	Current (A/m^2)	E_a kJ/mol	Kinetic parameters
[113]	Ni-YSZ-CeO_2 anode	$r_{CH_4} = \frac{K_1 K_2 K_3 p_{CH_4} p_{H_2O}}{(1 + K_2 p_{CH_4} + K_2 p_{H_2O})^2}$	973–1273	50	2–7	6000	≥ 18	–
[114]	Ni–ZrO_2 cermet	$r_{CH_4} = k_0 \exp\left(-\frac{E_a}{RT}\right)\left(1 - \frac{p_{CO} p_{H_2}^3}{p_{CH_4} p_{H_2O}}\right) p_{CH_4}$	973–1313	20	2.6–8	–	82	–
[115]	Ni cermet	$r_{CH_4} = k(p_{CH_4})^{1.5}$	1223	–	3	–		$k = 2.4e-3\ mol\ s^{-1} atm^{-1.25}$
[116]	Ni-YSZ cermet	$r_{CH_4} = k_0 \exp\left(-\frac{E_a}{RT}\right) p_{CH_4} (p_{H_2O})^{\alpha}$	1073–1273	50–80	2–7.4	–	17.8, 23.5	$k_0 = 490\ 4775\ mol\ g^{-1} h^{-1}$, $\alpha = -1.28, 1.25$
[86]	Ni-YSZ anode	$r_{CH_4} = k \frac{p_{CH_4}}{\left(1 + K_H p_{H_2}^{0.5} + K_S \frac{p_{H_2O}}{p_{H_2}}\right)^n}$	973–1273	55	1.2–7	–	135	$k_0 = 21\ mol\ bar^{-1} cm^{-2} s^{-1}$, $n = 2$
[117]	Ni/GDC, Au–Ni/GDC anodes	$r_{CH_4} = \frac{k_a p_{CH_4}}{1 + k \frac{p_{CH_4}}{p_{H_2O}}}$	1073–1173	57	0.25–1	2300	23–28	$k = 0.22 \sim 0.25$, $k_a = 15 - 45e-6$
[84]	Ni–$MgAl_2O_4$ cermet	$r_{CH_4} = \frac{\frac{k_1}{p_{H_2}^{2.5}}\left(p_{CH_4} p_{H_2O} - \frac{p_{CO} p_{H_2}^3}{K_1}\right)}{(1 + K_{CO} p_{CO} + K_{H_2} p_{H_2} + K_{CH_4} p_{CH_4} + K_{H_2O} p_{H_2O})^2}$	675–1000	15	3–5	–	240.1	–
[109]	Ni foil	$r = \frac{k p_{CH_4}}{1 + a \frac{p_{H_2O}}{p_{H_2}} + b\, p_{CO}}$	1073–1173	15	1–3	–	–	$a = 0.2 \sim 0.5$, $b = 0 \sim 2$
[91]	Ni–ZrO_2 anode	$r_{CH_4} = k_0 \exp\left(-\frac{E_a}{RT}\right)(p_{CH_4})^{\alpha}(p_{H_2O})^{\beta}$	1127–1180	–	1.53–2.5	–	95 ± 2	$\alpha = 0.85 \pm 0.05$, $\beta = -0.35 \pm 0.04$, $k_0 = 8542\ mol\ s^{-1} m^{-2} bar^{-0.5}$
[71]	Modified Ni–ZrO_2 anode	$r_{CH_4} = k_0 \exp\left(-\frac{E_a}{RT}\right)(p_{CH_4})^{\alpha}(p_{H_2O})^{\beta}$	1111–1195	–	1.4–3	–	20,8 ± 10	$\alpha = 1.4 \pm 0.01$, $\beta = -0.8 \pm 0.02$, $k_0 = 3.6e8\ mol\ s^{-1} m^{-2} bar^{-0.6}$
[92]	Ni-YSZ cermet film	$r_{CH_4} = k_{ad} p_{CH_4}\left(1 - \frac{k_{ad}}{k_r K_{H_2O}} \frac{p_{CH_4} p_{H_2}}{p_{H_2O}}\right)$	1073–1173	70	0.07–16	–	48.2 ± 2.1	$k = 3.44 \sim 23.5e-6\ mol\ kPa^{-1} s^{-1}$
[89]	Ni-CGO anode	$r_{CH_4} = k_0 \exp\left(-\frac{E_a}{RT}\right)(p_{CH_4})^{\alpha}(p_{H_2O})^{\beta}$	1073–1223	50	0–3	–	26.3	$k_0 = 4.05e-5\ mol/(s * m^2 * Pa^{1.19})$, $\alpha = 1.19$, $\beta = 0$
[89]	Ni-YSZ anode	$r_{CH_4} = k_0 \exp\left(-\frac{E_a}{RT}\right)(p_{CH_4})^{\alpha}(p_{H_2O})^{\beta}$	1073–1223	50	0–3	–	52	$k_0 = 4.05e-5\ mol/(s * m^2 * Pa^{1.19})$, $\alpha = 1.19$, $\beta = 0$
[118]	Ni-YSZ cermet	$r_{CH_4} = k_0 \exp\left(-\frac{E_a}{RT}\right)(p_{CH_4})^{a}(p_{H_2O})^{b}$	873–1023	60	2.5–5	–	117	$k_0 = 41.5\ mol\ g^{-1} s^{-1} bar^{-(a+b)}$, $a = 0.98$, $b = -0.09$
[118]	Ni-SDC cermet	$r_{CH_4} = k_0 \exp\left(-\frac{E_a}{RT}\right)(p_{CH_4})^{a}(p_{H_2O})^{b}$	873–1023	60	2.5–5	–	106	$k_0 = 40\ mol\ g^{-1} s^{-1} bar^{-(a+b)}$, $a = 0.98$, $b = -0.25$
[45]	Ni-GDC anode	$r_{CH_4} = k_0 \exp\left(-\frac{E_a}{RT}\right)(p_{CH_4})^{\alpha_{CH_4}}(p_{H_2O})^{\alpha_{H_2O}}$	973–1023	57	1.5–2.45	600, 1000	63–88	$k_0 = 1.1 \sim 18.9\ mol\ g^{-1} s^{-1} bar^{-(\alpha_{CH_4} + \alpha_{H_2O})}$, $\alpha_{CH_4} = 0.64 \sim 0.67$, $\alpha_{H_2O} = -0.04 \sim -0.08$
[79]	Ni-GDC anode	$r_{CH_4} = k_0 \exp\left(-\frac{E_a}{RT}\right)(p_{CH_4})^{\alpha_{CH_4}}(p_{H_2O})^{\alpha_{H_2O}}$	1043–1103	57	1.07–1.35	500–3000	50	$\alpha_{CH_4} = 0.15$, $\alpha_{H_2O} = 0.1$, *at open circuit, and both vary with increasing current*
[79]	Ni-GDC anode	$r_{CH_4} = k \cdot p_{CH_4} \frac{p_{H_2O}^a}{p_{H_2}^b} \frac{\left(1 - \frac{p_{CO} p_{H_2}^3}{K_1 p_{CH_4} p_{H_2O}}\right)}{\left(1 + K_{CH_4} p_{CH_4} + K_{H_2O} \frac{p_{H_2O}}{p_{H_2}}\right)^2}$	1043–1103	57	1.07–1.35	500–3000	160–220	$a = 0.007$, $b = 1.210$ *at open circuit, and both vary with increasing current*
[78]	Ni-GDC anode	$r_{MSR} = k\, p_{CH_4}^{\alpha} p_{H_2O}^{\beta} p_{H_2}^{\gamma}\left(1 - \frac{Q_{MSR}}{K_{MSR}}\right)$	973–1048	57	1.5–3	–	173.1	$\alpha = 0.8954$, $\beta = -0.0619$, $\gamma = 0.0693$, $k_0 = 9.472e8\ mol\ s^{-1} m^{-2} bar^{(\alpha+\beta+\gamma)}$
[78]	Ni-GDC anode	$r_{MSR} = k\, p_{CH_4}\left(1 - \frac{Q_{MSR}}{K_{MSR}}\right)$	973–1048	57	1.5–3	–	190.5	$k_0 = 9.472e8\ mol\ s^{-1} m^{-2} bar^{1}$
[78]	Ni-GDC anode	$r_{MSR} = \frac{k K_{CH_4} K_{H_2O} p_{CH_4} p_{H_2O}^{0.5}}{(1 + K_{CH_4} p_{CH_4}^{\alpha} + K_{H_2O} p_{H_2O}^{0.5})^2}\left(1 - \frac{Q_{MSR}}{K_{MSR}}\right)$	973–1048	57	1.5–3	–	207.6	$k_0 = 1.467e10\ mol\ s^{-1} m^{-2}$
[78]	Ni-GDC anode		973–1048	57	1.5–3	–	158.5	$k_0 = 2.787e7\ mol\ s^{-1} m^{-2} bar$

(*continued on next page*)

Table 1 (*continued*)

Ref	Anode Material	Rate Expression	T (K)	Wt% Ni	SC	Current (A/m^2)	E_a kJ/mol	Kinetic parameters
		$r_{MSR} = \frac{k p_{CH_4}}{\left(1 + K_{CH_4} p_{CH_4} + \frac{K_{H_2O} p_{H_2O}}{p_{H_2}}\right)^2}\left(1 - \frac{Q_{MSR}}{K_{MSR}}\right)$						
[82]	Ni-YSZ anode	$r = k_0 \exp\left(-\frac{E_a}{RT}\right) p_{CH_4}^{\alpha_{CH_4}}$	873–1073	51	1.5–6	250–1000	166.1	$k_o = 1.99e4\ mol\ s^{-1} m^{-2}\ Pa^{-0.7}$, $\alpha_{CH_4} = 0.56 \sim 0.80$,
[119]	Ni–ZrO_2–CeO_2 anode	$r_{CH_4} = k(p_{CH_4})$	1073–1123	5	2–4	–	39	$k = 2.6e9 \exp\left(-\frac{19500}{T}\right)\ \mu mol\ \min^{-1}$
[87]	Ni–α Al_2O_3 catalyst	$r_{CH_4} = r_1 + r_3\ (LH - HW\ type)$	748–823	15–17	3–7	–	209.2, 109.4	5.922e8, 1.093e3
[93]	Ni-based anode	Elementary reaction mechanism	1048–1223	–	1.5–4	0–80000	–	$k = AT^n \exp\left(-\frac{E_a}{RT}\right)\exp\left(\frac{\varepsilon_{CO9s0}\theta_{CO9s0}}{RT}\right)$
[94]	Ni-YSZ cermet	$r_{CH_4} = k_0 \exp\left(-\frac{E_a}{RT}\right)(p_{CH_4})^a (p_{H_2O})^b$	823–1023	60	2.5–6	–	121.3 ± 2.8	$a = 0.88 \pm 0.058$, $b = 0.083 \pm 0.039$, $k_0 = (6.472 \pm 1.921)e-3\ mol\ s^{-1} m^{-2} bar^{0.78}$
[95]	Ni-YSZ anode	$r_{CH_4} = k(p_{CH_4})$	873–1073	50	3	–	124	$k_0 = 1.82\ mol\ g^{-1} h^{-1}$
[96]	Ni–MgO catalyst	$r_{CH_4} = k(p_{CH_4})$	823–1023	7, 15	–	–	102	$k_0 = 2.5e5\ s^{-1} Pa^{-1}$
[81]	Ni coating on metal	$r = k p_{CH_4}\left(1 - \frac{p_{CO} p_{H_2}^3}{p_{CH_4} p_{H_2O} K_1}\right)$	723–873	75–85	2.87–5.53	–	226.4	$k_0 = 7.48e12\ mol\ bar^{0.5} kg_{cat}^{-1} s^{-1}$
[45]	Ni-GDC anode	$r_{CH_4} = k_0 \exp\left(-\frac{E_a}{RT}\right)(p_{CH_4})^{\alpha_{CH_4}} (p_{H_2O})^{\alpha_{H_2O}}$	923–1023	57	1.5–2.45	0	88 ± 11	$\alpha_{CH_4} = 0.64 \pm 0.15$, $\alpha_{H_2O} = -0.04 \pm 0.07$, $k_0 = 18.9 \pm 17.6\ mol/(\ bar^{0.60} s^{-1})$ 1.7 g catalyst
[45]	Ni-GDC anode	$r_{CH_4} = k_0 \exp\left(-\frac{E_a}{RT}\right)(p_{CH_4})^{\alpha_{CH_4}} (p_{H_2O})^{\alpha_{H_2O}}$	923–1023	57	1.5–2.45	632	63 ± 8	$\alpha_{CH_4} = 0.70 \pm 0.06$, $\alpha_{H_2O} = -0.04 \pm 0.03$, $k_0 = 1.1 \pm 0.9\ mol/(\ bar^{0.66} s^{-1})$ 1.7 g catalyst
[45]	Ni-GDC anode	$r_{CH_4} = k_0 \exp\left(-\frac{E_a}{RT}\right)(p_{CH_4})^{\alpha_{CH_4}} (p_{H_2O})^{\alpha_{H_2O}}$	923–1023	57	1.5–2.45	1052	66 ± 1	$\alpha_{CH_4} = 0.67 \pm 0.05$, $\alpha_{H_2O} = -0.08 \pm 0.05$, $k_0 = 1.5 \pm 0.2\ mol/(\ bar^{0.59} s^{-1})$ 1.7 g catalyst
[44]	Ni-YSZ anode	$r_{CH_4} = k_0 \exp\left(-\frac{E_a}{RT}\right)(p_{CH_4})^{\alpha_{CH_4}} (p_{H_2O})^{\alpha_{H_2O}}$	923–1048	57	1.83–5.50	0	59.27	$\alpha_{CH_4} = 0.50$, $\alpha_{H_2O} = -1.19$, $k_0 = 5.38\ mol/(\ bar^{0.69} g_{cat}^{-1} min^{-1})$
[44]	Ni-YSZ anode	$r_{CH_4} = k_0 \exp\left(-\frac{E_a}{RT}\right)(p_{CH_4})^{\alpha_{CH_4}} (p_{H_2O})^{\alpha_{H_2O}}$	923–1048	57	1.83–5.50	632	50.35	$\alpha_{CH_4} = 0.56$, $\alpha_{H_2O} = -0.59$, $k_0 = 7.43\ mol/(\ bar^{0.03} g_{cat}^{-1} min^{-1})$
[44]	Ni-YSZ anode	$r_{CH_4} = k_0 \exp\left(-\frac{E_a}{RT}\right)(p_{CH_4})^{\alpha_{CH_4}} (p_{H_2O})^{\alpha_{H_2O}}$	923–1048	57	1.83–5.50	1052	50.35	$\alpha_{CH_4} = 0.59$, $\alpha_{H_2O} = -0.49$, $k_0 = 14.29\ mol/(\ bar^{-0.10} g_{cat}^{-1} min^{-1})$
[44]	Ni-YSZ anode	$r_{CH_4} = k_0 \exp\left(-\frac{E_a}{RT}\right)(p_{CH_4})^{\alpha_{CH_4}} (p_{H_2O})^{\alpha_{H_2O}}$	923–1048	57	1.83–5.50	1052	50.35	$\alpha_{CH_4} = 0.59$, $\alpha_{H_2O} = -0.49$, $k_0 = 14.29\ mol/(\ bar^{-0.10} g_{cat}^{-1} min^{-1})$
[44]	Ni-YSZ anode	$r_{CH_4} = \frac{k \cdot p_{H_2}^c \cdot p_{H_2O}^b \cdot p_{H_2}^c \cdot \left(1 - \frac{p_{CO} p_{H_2}^3}{K_1 p_{CH_4} p_{H_2O}}\right)}{\left(1 + K_{CH_4} p_{CH_4} + K_{H_2O} p_{H_2O} / p_{H_2}\right)^2}$	923–1048	57	1.83–5.50	0	52.43	$a = 0.37$, $b = -1.03$, $c = -0.38$ $k_0 = 1.10\ mol/(\ bar^{1.04} g_{cat}^{-1} min^{-1})$
[44]	Ni-YSZ anode	$r_{CH_4} = \frac{k \cdot p_{H_2}^c \cdot p_{H_2O}^b \cdot p_{H_2}^c \cdot \left(1 - \frac{p_{CO} p_{H_2}^3}{K_1 p_{CH_4} p_{H_2O}}\right)}{\left(1 + K_{CH_4} p_{CH_4} + K_{H_2O} p_{H_2O} / p_{H_2}\right)^2}$	923–1048	57	1.83–5.50	632	41.73	$a = 0.45$, $b = -0.49$, $c = -0.04$ $k_0 = 2.37\ mol/(\ bar^{0.08} g_{cat}^{-1} min^{-1})$
[44]	Ni-YSZ anode	$r_{CH_4} = \frac{k \cdot p_{H_2}^c \cdot p_{H_2O}^b \cdot p_{H_2}^c \cdot \left(1 - \frac{p_{CO} p_{H_2}^3}{K_1 p_{CH_4} p_{H_2O}}\right)}{\left(1 + K_{CH_4} p_{CH_4} + K_{H_2O} p_{H_2O} / p_{H_2}\right)^2}$	923–1048	57	1.83–5.50	1052	43.55	$a = 0.43$, $b = -0.34$, $c = -0.02$ $k_0 = 4.07\ mol/(\ bar^{-0.07} g_{cat}^{-1} min^{-1})$

Table 2
WGS kinetic models over various catalysts.

REF	Catalyst material	Rate Expression	Temperature (K)	Wt% Ni	SC	Current density	Kinetic Parameters
[120]	Iron and Copper-based	$r_{WGS} = \frac{K_0 P_{CO} P_{H_2O}\left(1-\frac{P_{CO_2}P_{H_2}}{P_{CO}P_{H_2O}K_e}\right)}{\left(1+K_1P_{CO}+K_2P_{H_2O}+K_3P_{CO_2}+K_4P_{H_2}\right)^2}$	673–973	–	–	–	$k_0 = 0.92\ mmol\ g^{-1}s^{-1}atm^{-2}$ $E_{ao} = 4080\ J\ mol^{-1}$ $k_1 = 2.21 mmol\ g^{-1}s^{-1}atm^{-2}$ $E_{a1} = -910\ J\ mol^{-1}$ $k_2 = 0.4\ mmol\ g^{-1}s^{-1}atm^{-2}$ $E_{a2} = -1420\ J\ mol^{-1}$ $k_3 = 0.0047\ mmol\ g^{-1}s^{-1}atm^{-2}$ $E_{a3} = -24720\ J\ mol^{-1}$ $k_4 = 0.052\ mmol\ g^{-1}s^{-1}atm^{-2}$ $E_{a4} = -14400\ J\ mol^{-1}$
[121]	Ni-YSZ	$r_{WGS} = K_{sf}\left(P_{H_2O}P_{CO} - \frac{P_{H_2}P_{CO_2}}{K_{ps}}\right)$	523–1073	–	0.35–6	7300	$K_{sf} = 0.0171\exp\left(-\frac{103191}{RT}\right)\ mol\ m^{-3}\ Pa^{-2}s^{-1}$ $K_{ps} = \exp(-0.2935Z^3 + 0.6351Z^2 + 4.1788Z + 0.3169)$
[122]	Cu/ZnO/Al_2O_3	$r_{WGS} = k_0\exp\left(-\frac{E_a}{RT}\right)\left(P_{CO}P_{H_2O} - \frac{P_{CO_2}P_{H_2}}{K_e}\right)$	373–673	–	1–3	–	$E_a = 47.4\ kJ\ mol^{-1}$ $k_0 = 2.96{\cdot}10^5\ mol\ hr^{-1}\ Pa^{-2}$
[45]	Ni-YSZ and Ni-SDC	$k_{eq,WGS} = \exp\left(-\frac{\Delta G_{wg}}{RT}\right)$	1073–1223	–	0–3	0–6000	–
[123]	Fe_2O_3/Cr_2O_3/MgO	Elementary reaction mechanism	473–723	–	–	–	It varies at different steps
[124]	Ni	$r = kp_{CO}^l p_{H_2O}^m p_{CO_2}^n p_{H_2}^q\left(1-\frac{p_{CO_2}p_{H_2}}{K_{eq}p_{CO}p_{H_2O}}\right)$	573–1273	–	–	–	$k_0 = 8e6\ s^{-1}$, $E_a = 85\ kJ\ mol^{-1}$
[124]	Ni-ceria	$r = kp_{CO}^l p_{H_2O}^m p_{CO_2}^n p_{H_2}^q\left(1-\frac{p_{CO_2}p_{H_2}}{K_{eq}p_{CO}p_{H_2O}}\right)$	573–1273	–	–	–	$k_0 = 1.7e8\ s^{-1}$, $E_a = 85\ kJ\ mol^{-1}$
[125]	Green NiO	$r = kp_{CO}^x p_{H_2O}^y p_{CO_2}^z$	523–553	–	–	–	$E_a = 15-20\ kcal\ mol^{-1}, x = 0-0.7, y = 0-0.3$
[125]	Black NiO	$r = kp_{CO}^x p_{H_2O}^y p_{CO_2}^z$	535–553	–	–	–	$E_a = 23\pm1\ kcal\ mol^{-1}$, $x = 0.4-0.8$, $y = 0$, $z = -0.4$
[105]	Ni–Al_2O_4/MgO_2	$r = \frac{k_H p_{CO}^a p_{H_2O}^b}{p_{H_2}^c}$	673–873	40	4	–	$k_{H0} = 5.49e6\ s^{-1}bar^{-1}$, $E_a = 83.7\ kJ\ mol^{-1}$, $c = -\frac{1}{07}-0.55$, $a = 1.04$, $b = -0.03-1.01$
[126]	Ni–Al_2O_3	$r = kc_{CO}c_{H_2}^{0.3}$	1069–1112	11	3–5	–	$k_0 = 3100\ m^{3.9}\ kg^{-1}s^{-1}\ mol^{-0.3}$, $E_a = 82\ kJ\ mol^{-1}$
[127]	Ni–Re	$r = k_2 p_{CO}^a p_{H_2O}^b p_{H_2}^c p_{CO_2}^d\left(1-\frac{p_{H_2}p_{CO_2}}{K_{eq}P_{CO}P_{H_2O}}\right)$	573–673	–	0.6–1	–	$k_{20} = 2.55e-6$, $E_a = 33.48\ kJ\ mol^{-1}$, $a = 1.9645$, $b = 1.9645$, $c = 4.2979$, $d = -9.4584$
[53]	Ni–CeO_2	$r = k\left(y_{CO}y_{H_2O} - \frac{y_{CO_2}y_{H_2}}{K_{eq}}\right)$	523–873	5–12.5	–	–	$lnk_o = 5.241\pm1.6$, $E_a = 42.51\pm7.9$

remainder being CO_2. This variation means that the energy content of biogas can vary; the lower heating value (LHV) is between 16 MJ/m^3 and 28 MJ/m^3. In addition, raw biogas often contains considerable quantities of undesirable trace compounds such as hydrogen sulphide and siloxane that can cause SOFC degradation at low concentrations. The amounts of methane and trace contaminants vary significantly on the working condition of the production unit and the feeding biomass composition [3,14].

However, the viability of using biogas in SOFCs has not been systematically and comprehensively investigated. Therefore, recent progress in the effective utilization of biogas in SOFCs is reviewed for H_2 and power productions. Perspectives for the current advances, challenges, and the direction of future work are also discussed in this section.

4.1. Power production

The direct utilization of hydrocarbons in a SOFC was first reported by Park et al. [142–144] as early as 1995 but the power density reported was low. Murray et al. [145] reported a direct Methane-Solid Oxide Fuel Cell (CH_4–SOFC) without carbon deposition when a 0.5 μm thick (Yttrium Oxide)$_{0.15}$(Cerium (IV) Oxide)$_{0.85}$(Yttria Doped Ceria) ($(Y_2O_3)_{0.15}(CeO_2)_{0.85}$(YDC)) porous film was applied between the Ni-YSZ anode and YSZ electrolyte.

Lanzini et al. [146] investigated the behaviour of planar SOFCs fed by two simulated biogas compositions coming from anaerobic digestion, namely bio-hydrogen (bio-H_2) and bio-CH_4. Ni-YSZ anode-supported cells and Ni-GDC anode electrolyte-supported cells were used. The oxidant addition was shown to help prevent carbon deposition and accelerate CH_4 conversion into H_2. Furthermore, the cell voltage was stable when loads of 0.5 mA/cm^2 and 0.3 mA/cm^2 were applied to the anode-supported and electrolyte-supported cells, respectively, for at least 50 h at 800 °C. This study developed an energy model of a complete SOFC system operating on reformed bio-CH_4. The steam-reformed CH_4 demonstrated the best performance, with more than 41% electrical efficiency.

The performance of three configurations of biogas-fuelled SOFC Micro-Combined Heat and Power (micro-CHP) systems for residential applications has been evaluated by Farhad et al. [147]. Three configurations with anode off-gas recirculation, steam reforming, and partial oxidation were investigated in this study. Depending on the size, location, building type, and design of a residential unit, these systems may be able to provide the domestic hot water and electric power requirements of the unit. A sensitivity analysis of the cell operating voltage, the fuel utilization, the CHP efficiency, the biogas fuel composition, excess aid to control the stack temperature, and the thermal to electric ratio was conducted through a detailed analysis. According to the findings, the optimum cell voltage is higher than the cell voltage at which the SOFC stack's minimal number of cells is obtained. Furthermore, the exergy analysis revealed that the systems under consideration have a significant potential for generating additional electric power, particularly if the partial oxidation system is integrated with other power generation devices and adjusted suitably. However, the sensitivity analysis of the partial oxidation on the system performance was missing in this study for an accurate evaluation of such systems.

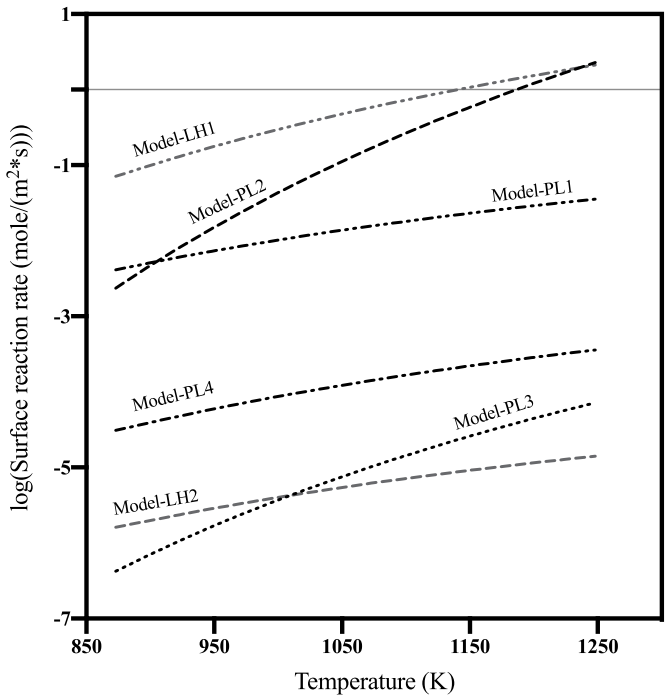

Fig. 6. The methane steam reforming reaction rates versus temperature on Ni-YSZ anodes. The six selected models are: Model PL-1 ([89]), Model PL-2 ([90]), Model PL-3 ([95]), Model PL-4 ([44]), Model LH-1 ([86]), Model LH-2 ([44]).

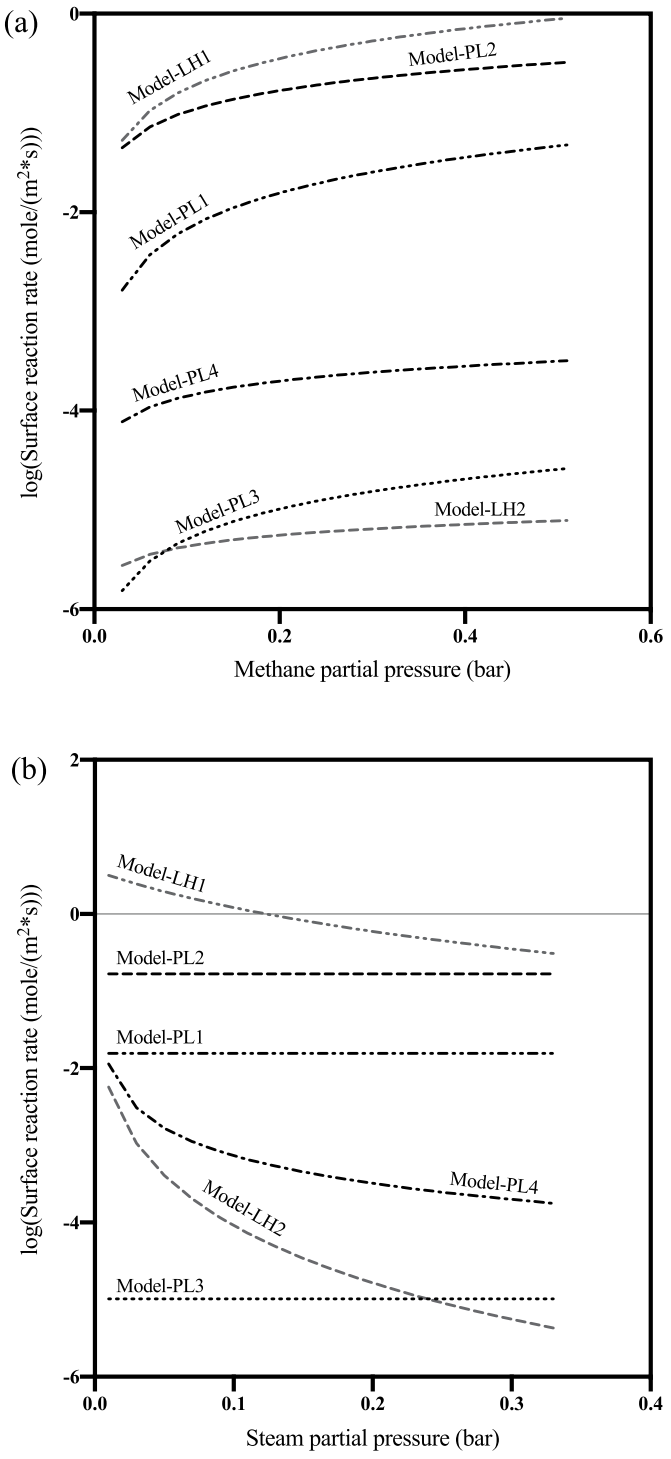

Fig. 7. (a) The methane steam reforming reaction rates versus methane partial pressure on Ni-YSZ anodes; (b). The methane steam reforming reaction rates versus steam partial pressure on Ni-YSZ anodes. The 6 six selected models are: Model PL-1 ([89]), Model PL-2 ([90]), Model PL-3 ([95]), Model PL-4 ([44]), Model LH-1 ([86]), Model LH-2 ([44]).

The direct application of biogas in an anode-supported SOFC can give good MSR performance and assure high conversion of CH_4 even when the temperature is much below the nominal value. Santarelli et al. [66] investigated the direct reforming of biogas on Ni-based SOFC anodes experimentally. A mathematical model comprising the reforming kinetics on Ni catalysts was utilised to forecast the gas composition profile across the fuel channel. The operational maps of a fuel cell based on direct reforming of biogas were developed. Experiment-derived polarization curves were used to validate the model.

A biogas-fed decentralized SOFC combined heat and power (CHP) system model, consisting of a pre-reformer, an SOFC stack, an afterburner and a heat-recovery boiler, was proposed and analyzed by Wang et al. [57]. The system model integrates a multi-scale hierarchical 3D SOFC stack model with 0D balance of power (BoP) component models, enabling simultaneous investigations of the overall system performance and the stack-internal distributed properties down to the electrode scale. The effects of steam to carbon ratio, biogas composition and operation voltage of the SOFC stack on the electrical and CHP efficiencies of the system and the temperature gradient within the SOFC stack were studied. The proposed system model is an insightful and powerful tool for designing hybrid SOFC combined heat and power systems. However, the stack durability may decrease with increasing CH_4 in biogas due to the increase of both the temperature gradient and the carbon coverage on the electrodes. Furthermore, the increase in operating voltage leads to a decrease in the system electrical efficiency and the stack temperature gradient but an increase in the system CHP efficiency.

The power generation using CH_4 in SOFCs has been widely researched and applied. However, power density may improve by modifying the fuel cell geometry or designing better anode materials. The power density of SOFC fuelled with humidified CH_4 has been increased fast from 50 mW/cm^2 at 700 °C on Ni-YSZ anode and 150 mW/cm^2 on the Nickel–Cerium (IV) Oxide-Yttria-Stabilized Zirconia (Ni/CeO_2/YSZ) anode [143] in 1999 to 640 mW/cm^2 at 900 °C on the Ni-Scandia Stabilized Zirconia (ScSZ) zirconia anode in 2004 [148]. A power density of 545 mW/cm^2 was achieved with 30% CH_4 on micro-channelled Ni-GDC anode support as it provides a rapid gas diffusion pathway [48]. A SOFC with a Ni-YSZ anode and Nickel/Cerium (IV) Oxide-Aluminum Oxide (Ni/CeO_2–Al_2O_3) layer achieved a power density of 830 mW/cm^2 with 25% CH_4/25% CO_2/Ar at 800 °C [149]. Recently, cells with samarium modified Ni-YSZ anode operated on humidified CH_4 reached a power density of 1540 mW/cm^2 at 800 °C [150]. A complete understanding of the kinetics of various anode material properties helps realize the efficient yet safe application of biogas in

SOFCs. However, this current review will not discuss the anode materials, and the readers can refer to other reviews from different perspectives [16,39,51,128–132].

4.2. Hydrogen/syngas and power co-production

Although many technologies for green H_2 production are inefficient and non-competitive with conventional methods, SOFC technology stands out as a potent alternative. Co-generation of electricity and syngas from CH_4 via SOFCs to reach high combined efficiency and achieve zero-emission is highly attractive to enhance the cost-effectiveness of biogas utilization. However, achieving high power output and syngas formation rates with sufficient operational stability remains a significant challenge in existing SOFCs.

A prototype SOFC reactor with microchannel reactors integrated into the anode has been designed to directly co-generate power and syngas from CH_4. Fan et al. [151] demonstrated effective co-generation by incorporating a catalytic microchannel reactor into the anode. The integrated anode contains distinct dendritic channels filled with a highly efficient nanofibrous Ni-based composite (Ni/CeO_2–Al_2O_3) that serves as an internal catalytic bed reformer. The novel SOFC anode structure successfully displays thermal and material coupling effects between the exothermal fuel oxidation and endothermal reforming reactions. Compared to the conventional SOFCs, the peak power density was enhanced by 25% and the syngas production and duration of stable operation by more than twice. The new SOFC architecture has a lot of practical uses. The co-generation performance can be increased further by optimizing the electrochemical oxidation of fuels and CH_4 reforming in future experiments, which may be accomplished by adjusting the anode support thickness. The combined SOFC reactor with high energy conversion efficiencies is promising for the application of the alternative solid oxides cell-based electrochemical fuel conversion systems.

Auto thermal reforming of CH_4 integrated with exothermal POM, endothermal MSR, and DMR can achieve a high overall thermal efficiency. It can be utilised in conjunction with SOFCs to eliminate the requirement for oxygen while also avoiding the safety risks associated with CH_4/O_2 mixtures. In addition, electrical power is generated together with heat. An investigation on auto thermal reforming of CH_4 over an integrated SOFC reactor for power and syngas co-generation was conducted by Fan et al. [149]. The efficient electrochemical auto thermal reforming of CH_4 over a SOFC with the catalyst beds within an anode channel configuration was demonstrated. The catalyst bed configuration increased the syngas yield significantly by improving the CH_4 conversion and selectivity towards syngas. The increased fuel accessibility shows improved mass transport at the electrode-electrolyte interface, aided by integrated catalyst beds. The catalyst beds are more efficient at catalyzing CH_4 reforming than a traditional catalyst layer on the anode surface. Following initial cell microstructure stabilization, the SOFC reactor demonstrated consistent cell performance and syngas output during a 120-h test, with no detectable carbon deposition.

Panagi et al. [152] used SOFCs to produce highly efficient electrical power and syngas from bio-hythane, a gaseous mixture consisting of 60/30/10 vol% $CH_4/CO_2/H_2$ produced through an improved two-stage anaerobic digestion (AD) process. Fuelling SOFCs with bio-hythane has been experimentally demonstrated to co-produce electricity and valuable chemicals. The increases in SOFC efficiency have shown an increase in energy yield from the two-stage AD process compared to single-stage AD in SOFCs. The presence of H_2 in bio-hythane resulted in up to 77% higher overall electrical energy yields from biomass. The maximum power density of a bio-hythane-fuelled SOFC was around 160 mW/cm^2 and may be improved further by modifying the bio-hythane composition. The findings show that bio-hythane generation, rather than biogas, can be a more cost-effective way to generate electricity from biomass. Many items have been successfully coproduced. The technologies described in this study could be utilised to dispose of and add value to a wide range of challenging renewable and industrial waste gas streams in the future.

In the past 20 years, modelling studies on such systems have made the system evaluation quicker, cheaper, and safer, beneficial to the experimental studies. Combined CH_4 reforming with CO_2 and H_2O in proton-conducting SOFCs (H–SOFCs) for syngas/power co-generation was studied by Chen et al. [50], and the effects of adding H_2O to the CO_2 and CH_4 fuel mixture on the performance of a tubular proton-conducting SOFC were studied numerically. The results show that the CH_4 conversion and current density were improved after adding H_2O to the fuel. Furthermore, sensitivity studies indicate that H_2O addition can effectively control the H_2:CO ratio and that H_2 starvation can be alleviated, especially at high current density conditions.

Both numerical and experimental analysis of the biogas reforming process on the Ni-YSZ catalyst was carried out by Brus et al. [94,118]. A numerical model containing MSR, DMR, and WGS reactions was proposed to predict the composition of the gas mixture at the outlet of the reformer. Different thermal boundary conditions, steam to carbon ratios, and fuel compositions were examined. The modelling results agreed with the experimental results and successfully predicted the outlet H_2 composition under different operating conditions.

Another thermal-electrochemical modelling study on the syngas and power co-generation from H–SOFC assisted by DMR was conducted by Chen et al. [65]. The coupled heat and mass transport with electrochemical and chemical reactions were fully considered, and the co-generation performance was numerically characterized. Advantages have been shown by integrating the H–SOFC process with the internal DMR process for power and syngas co-generation using GHGs.

Under its “Green Village” program, Delft University of Technology has the initiative to build a power plant (car parking lot) with the fuel cells used in vehicles for personal mobility. Exergy analysis of different system designs on the fuel cell electric vehicle as a power plant and SOFC as a natural gas reformer was conducted by Fernandes et al. [153] in 2016. The tri-generation system generates power, heat, and H_2. The system is divided into three zones: H_2 production, parking, and a pumping station, as shown in Fig. 8. This study evaluates four different system designs in two different facility operation modes: (a) the car as power plant (CaPP) mode, which corresponds to the open period of the facility and uses fuel cell electric vehicles (FCEVs) for electricity and water production while parked; (2) the pump mode, which compresses H_2 and pumps it to the vehicle’s fuel tank. The present catalytic reformer (CR) and a SOFC acting as a reformer (SOFCR) differ in terms of reforming technology, as well as the option of combining carbon capture and storage (CCS). The results show that the SOFCR unit greatly minimizes exergy destruction, resulting in a 20% efficiency improvement in SOFCR-based system designs in both operating modes compared to CR-based system designs. It also mitigates the system efficiency reduction to only 2% by integrating a CCS unit, whereas CR-based systems have a 7–8% efficiency reduction. In Pump mode, the SOFCR-based system has a 60% tri-generation efficiency. In addition, the use of bio-CH_4 in these systems can easily be expanded.

An afterburner-powered CH_4 steam reformer for SOFC application was numerically studied by Mozdzierz et al. [154] in 2018. A 0D model of an after burner-powered fuel cell with a reformer has been developed to investigate the effect of fuel composition on SOFC performance. It is proven that SOFC can thermally support the H_2 production system if a heat exchanger-type MSR reactor is adopted. One possible application for an after burner-heated reformer is to feed the syngas produced during the reforming process in a SOFC. The high steam to carbon ratio, which is not always desirable for the MSR, positively affects cell efficiency.

In theory, any combustible fuel can generate electrical power and H_2 in SOFCs. Gorte et al. [155] investigated the potential of ethane, 1-butene, *n*-butane, and toluene as fuels for SOFCs. Reformed liquid hydrocarbons like dodecane and diesel have also been reported as good fuels for SOFCs [156,157]. Reformed bio-diesel was also evaluated as a potential fuel for SOFCs by Mehrpooya et al. [158]. However, the fuel

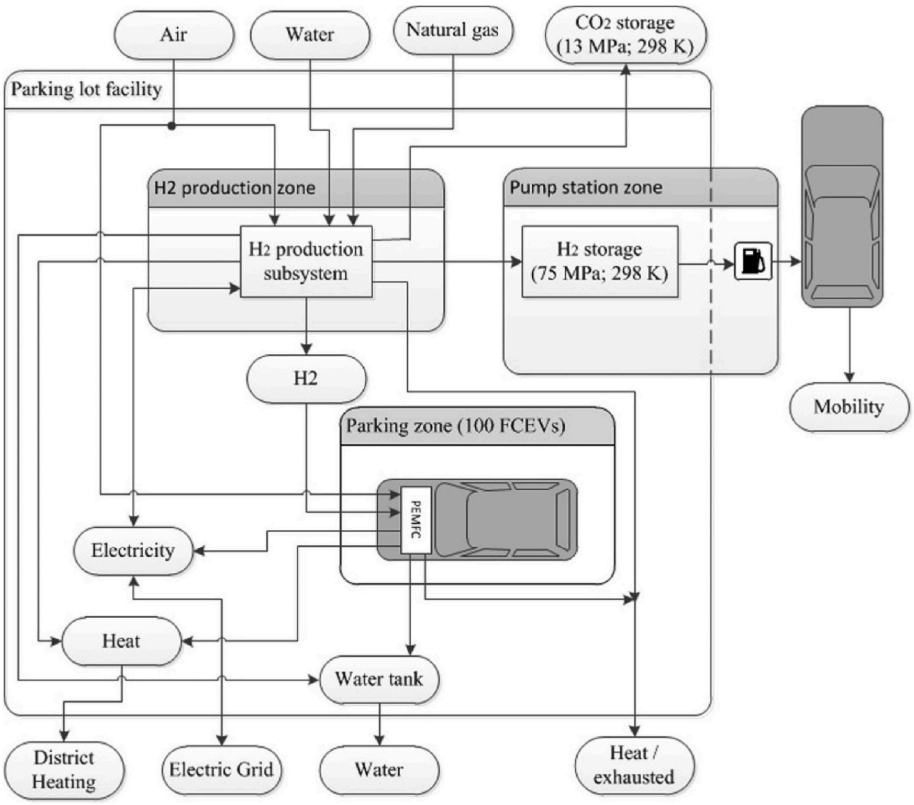

Fig. 8. The layout of the 'car as a power plant facility and flow diagram of inlet and outlet streams ((Reprinted with permission from Ref. [153], Copyright (2016), Elsevier).

cell degradation is higher than H_2-fed SOFC [159].

Leone et al. [160] investigated the performance and the degradation issues of CH_4-free biogas fuelled directly to a Ni-based anode-supported SOFC. The CH_4-free biogas is produced using an innovative process. Biomass is fermented with a pre-treated bacteria inoculum (Clostridia), which can completely inhibit the mechanization step during fermentation and thus produce an H_2/CO_2 mixture rather than the traditional CH_4/CO_2 anaerobic digester gas (bio-CH_4). Despite the considerable amount of sulphur in the fuel stream, the fuel cell produced an acceptable power output (at 800 °C, 0.35 W/cm^2 with biogas against 0.55 W/cm^2 with H_2). A short-term test with as-produced biogas demonstrated that sustainable biomass processing created biogas can be directly fed into SOFCs using typical anode materials with no carbon deposition, eliminating the requirement for a pre-reformer. Teramoto et al. [20] investigated CH_4-ammonia (NH_3) mixed fuel direct reforming on Ni-YSZ anode crushed materials. The reaction kinetics of combined fuel reforming/decomposition was explored experimentally. NH_3 decomposition takes priority, while MSR only becomes active after enough NH_3 has been consumed. As a result, the CH_4 to NH_3 ratio in the mixed fuel can be adjusted to control local temperatures. At a specific combined ratio, a H_2 production rate was greater than pure CH_4 or NH_3.

SOFCs have been promoted as an alternative to convert biogas into electricity and heat with high efficiency. However, few studies have considered using the anode exhaust gas to co-produce green H_2 together with electricity and heat, which could increase the performance and profitability of these systems. Thus, Nakashima et al. proposed a new approach to model SOFC with direct internal reforming to produce power, H_2 and heat [35]. The results indicate that the proposed system can reach exergy efficiencies between 57% and 69% depending on the CH_4 content of biogas. Furthermore, H_2 separation reduces the amount of fuel to be burned. In addition, significant performance improvements can be achieved by optimizing the H_2 recovery of the pressure swing adsorption and the SOFC operating temperature.

A new configuration of an integrated SOFC and gas turbine (GT) combined with a biogas reforming cycle for the cogeneration of power and H_2 was proposed by Soleymani et al. [34]. The thermal energy discharged from the SOFC-GT system is used to supply the energy required for the reforming reaction in the biogas reforming cycle for H_2 production. A parametric study has been performed to demonstrate the effect of different parameters on the main performance metrics of the devised system. The results revealed that the energy efficiency and exergy efficiency of the proposed combined system have increased compared to the SOFC-GT system by 23% and 28%, respectively. As a result, the net output power and H_2 production rate are obtained by 2726 kW and 0.075 kg/s, respectively.

A biogas-based poly-generation system for the combined H_2, heat and electricity production was designed and analyzed from energy and economic points of view by Mimutillo et al. [161]. The system consists of four sections: a biogas processing unit consisting of an auto thermal reactor and a water gas shift reactor, an SOFC power unit, a H_2 separation unit and a compression/storage unit. The syngas generated in the autothermal reforming reactor is split into two fluxes. The first one is sent to the SOFC power unit for electricity and heat generation. The second one is sent to the WGS reactor to increase the H_2 content. The system behaviour and the energy performances were investigated by the numerical simulation based on thermo-electrochemical models. Four operating conditions related to different SOFC loads (from 30% to 100%) have been analyzed. The evaluated overall efficiencies range from 68.5% to 72.3%, and the energy-saving, calculated for the separate production of H_2, heat and electricity, ranges from about 8% to 26%. Therefore, the biogas polygene ration system can present an alternative solution to operating the existing biogas power plant being more profitable to produce H_2 in the near future when the incentives for renewable electric power are not available.

Hydrogen energy systems are essential components of solutions toward reducing the negative consequences of global warming. Hydrogen

should be affordable, reliable, safe, clean, and efficient for a sustainable future. Evaluation of the technical, environmental, social, and economic performance of such systems is critical for developing reliable hydrogen production and application [8,10,13,16,35,38,162–165]. By selecting the most sustainable source for hydrogen production and storage systems and enhancing the performance of hydrogen end-user technologies such as fuel cells, the demand for fossil fuels for hydrogen energy production could be reduced. Different hydrogen production sources and systems and some hydrogen storage options are comparatively investigated in detail by Acar et al. [166]. Biomass, geothermal, hydro, nuclear, solar, and wind are the selected hydrogen production sources; biological, thermal, photonic, and electrical are the selected hydrogen production methods; and chemical hydrides, compressed gas, cryogenic liquid, metal hydrides, and nanomaterials are the selected hydrogen storage systems. The economic, environmental, social, and technical performance and reliability of the chosen options are compared, providing a broader sustainability investigation of hydrogen production and storage together. A more in-depth discussion on the effectiveness and difficulties of hydrogen production is not included in this review but can be found elsewhere [5,13,15,55,163,167,168].

4.3. Advances and challenges

SOFCs provide a feasible alternative to the conventional energy conversion processes due to their highly efficient and eco-friendly operation. The high operating temperature (800–1000 °C) of SOFCs, oxide-ion conduction through the electrolyte, and the catalytic activity of the anode material for reforming reaction enable them to operate with a wide range of hydrocarbons. All techniques developed to produce H_2 through CH_4 reforming can be easily applied for internal reforming in SOFCs to enable carbon-neutral H_2 production ultimately. The reforming process can occur internally in the SOFC itself or externally in a catalytic (pre-) reformer. Because SOFCs operate at high temperatures, the electrode polarization losses are often much lower than those observed in their low-temperature equivalents, resulting in significantly lower energy consumption. Furthermore, compared to low-temperature devices based on proton-conducting electrolytes, SOFCs based on O^{-2} conductors offer significantly higher fuel flexibility.

CH_4 reforming occurring directly on the SOFC anodes enables a less complicated system with a high overall thermal efficiency at a lower cost [153]. The current main focus of CH_4-fed SOFC operations is to increase the durability and stability of the SOFC systems and maximise the H_2 and power productions [42,169]. Issues like the fabrication and electrode materials costs [170,171], microstructural changes or degradations of anode materials during operations [172], defect segregation [173–175], insufficient current collection [176,177] and high cost for interconnect materials and fabrication [178–180] and the system design [181–183] are common to all SOFCs, regardless of the fuels. Therefore, these topics are not expanded in this review, and the interested readers can refer to the reviews by Shi et al. [184], Faes et al. [172], Badwal et al. [185,186], Tao et al. [39,134,187] and Gorte et al. [131,132,188,189].

Biogas is a renewable energy source composed of CH_4, CO_2, and other trace compounds produced from organic matter's anaerobic digestion. Various feedstocks combined with different digestion techniques yield biogas with different compositions. Biogas derived from various biomass would be the perfect fuel for SOFCs if sufficiently clean. However, trace contaminants in the biogas vary on the biomass sources, and the treatment conditions can cause the degradation or failure of such systems. For example, municipal waste biogas contained elevated volatile chemical products such as aromatic hydrocarbons, siloxanes, and halogenated hydrocarbons. Food waste biogas contained high sulphur-containing compounds, including hydrogen sulphide, mercaptans, and sulphur dioxide. Biogas produced from dairy manure generally had lower concentrations of trace chemicals, but the combustion products had slightly higher toxicity responses than the other feedstocks [3,6,10,14,190,191]. Efficient and cost-effective gas cleaning measures are crucial for the widespread application of such systems, which requires knowledge of the effect of the contaminants on the fuel cell performance and the tolerance limits on the anode. However, the effects of these contaminants on the fuel cell operation are not the focus of the current review and will not be discussed in-depth. Hydrogen production via dry biogas reforming, including the preparation of catalysts, the optimization of operation conditions, and the influence of impurities in biogas, has been reviewed by Gao et al. [192]. In addition, newer reactors, including membrane reactors, microreactors, and solar thermal flow reactors, were reviewed. However, the effects of various impurities in biogas on dry reforming require further study, including the mechanism of H_2S and siloxane poisoning and the development of poisoning-resistant catalysts. Almost all research on dry biogas reforming has used simulated biogas as the feed gas. Future research should test dry reforming using actual biogas, an essential step to push this technology toward practical applications. A detailed review of the strategies for carbon and sulphur tolerant SOFC materials, including the conventional CH_4 reforming catalysts and novel SOFC anode materials, has been conducted by Boldrin et al. [193]. Furthermore, the interested readers can refer elsewhere for more detailed information on the advances in biogas cleaning techniques [24,60,68,194,195].

The application of current can mitigate the carbon deposition and sulphur poisoning effect on the anode materials, which is the unique advantage for CH_4 reforming in SOFCs. However, The interaction of the electrochemical reactions and the CH_4 reforming reaction, which is essential for understanding the actual reforming process in biogas-fed SOFCs [8,50,58,60,105,159], is rarely reported and often overlooked.

The effect of the electrochemical reaction on the reforming activity was first experimentally investigated by Nakagawa et al. [113] over the Ni-YSZ-CeO_2 anode. An LH-HW rate equation was proposed for the open-circuit working condition. A catalytic activity deterioration was observed with low p_{H_2}, high p_{H_2O} and high current density, possibly because of the oxidation of the Ni surface by the oxygen ions (O^{2-}) or H_2O. However, no extensive investigation into the effects of current on the reforming reaction kinetics has been conducted.

The catalytic behaviour of Nickel–Zirconium Dioxide-Cerium (IV) (Ni–ZrO_2–CeO_2) anode in SOFCs was investigated by Belyaev et al. [112,119] and how the electrochemical pumping of O_2 to or from the reaction zone influences the MSR reaction was reported. A linear increase in reaction rate with CH_4 concentration was observed. However, the anodic and cathodic polarization of the Ni–ZrO_2–CeO_2 anode did not significantly influence the reforming reaction rate.

Timmermann et al. [89] reported PL rate expressions of MSR reaction over Ni-YSZ and Ni-CGO anodes. The MSR reaction was independent of H_2O, and the dependence of CH_4 was slightly higher than 1. The reforming reaction has reached equilibrium at the outlet at 950 °C. They have also claimed that less than stoichiometric ratios of steam to carbon could be used under electrical load at the sacrifice of the lack of water.

Fan et al. [44,45] extended this study in which PL and LH kinetic models were used to determine and analyse the MSR reaction rate under various operating conditions. The electrochemical reaction and anode thickness effects were investigated to obtain accurate rate expressions for biogas-fed SOFC modelling studies. The findings of the study suggest that the intricacy and versatility of these models vary, and some are better at simulating real-world behaviour than others. Furthermore, since the experimental data reported were obtained under non-identical operating conditions, such as catalyst loading and feed gas composition, thus cannot be directly applied to other studies.

Additionally, the direct internal reforming of CH_4 may also prompt high-temperature gradients within the SOFC, resulting in the local thermal stresses, which accelerate cell degradation. Recent work has shown that such thermal stress severity depends on the CH_4 concentration in the fuel gas and the kinetics of electrochemical and MSR reactions. Therefore, developing an appropriate kinetic expression for the

MSR reaction over the Ni-GDC anodes within the SOFC is highly beneficial in predicting accurate temperature and concentration profiles within the fuel cell and, ultimately, the safe operation, design, and development of SOFCs.

5. Perspectives and future work

Biogas is an abundant renewable energy source produced by anaerobic treatment of biological waste such as sewage sludge, agro-industrial, and industrial animal waste. Utilizing biogas instead of fossil fuels in a solid oxide fuel cell (SOFC)-based system is an excellent choice to achieve a fossil-free and sustainable energy future. Biomethane is a near-pure source of methane produced either by upgrading biogas or through the gasification of solid biomass followed by methanation. Biomethane has an LHV of around 36 MJ/m^3. It is extremely similar to natural gas; therefore, it can be used without changes in transportation and distribution infrastructure, end-user equipment, and natural gas vehicles.

This review provides insights into the catalytic process of methane reforming in SOFCs. This work helps formulate appropriate kinetic models from experimental studies to aid modelling studies of the direct application of methane in SOFC systems. However, the kinetic models and the kinetic parameters for the methane reforming reaction are still under debate, especially regarding the influence of steam concentration on the overall reaction rate. Furthermore, the fundamental principles underlying the effects of the electrochemical reaction on steam dependency have yet to be explained, necessitating further research into the effect of the electrochemical reaction on reforming kinetics. To understand the impact of anode (micro-)structure on reforming kinetics, the mass transfer should be considered, and a more extensive current density range should be implemented. Future research on developing the novel anode catalyst should also be done to facilitate the direct application of biogas in the SOFCs for H_2 and electricity production.

Declaration of competing interest

The authors declare that they have no known competing financial interests or personal relationships that could have appeared to influence the work reported in this paper.

Acknowledgments

The authors would like to thank Mr. Riley Coleman, Mr. Elwyn Omanga, Mr. Ben Britt, Beatrix Nessia Kamadjaja (James Cook University, Australia), and Ms. Himanshi Shrivastava (Indian Institute) of Technology, Delhi, India.) for their considerable effort in the content collection. The authors also would like to thank Elsevier and MDPI for permitting the figure citations.

Nomenclature

Abbreviations

GHG	Greenhouse gases
FCH-JU	European Fuel Cells and Hydrogen Joint Undertaking
MSR	Methane Steam Reforming
WGS	Water Gas Shift
DMR	Dry methane reforming
SOFCs	Solid Oxide Fuel Cells
DIR	Direct Internal Reforming
DIR-SOFCs	Direct Internal Reforming-Solid Oxide Fuel Cells
CH_4–SOFC	Methane-Solid Oxide Fuel Cells
$(Y_2O_3)_{0.15}(CeO_2)_{0.85}$(YDC)	(Yttrium Oxide)$_{0.15}$(Cerium(IV) Oxide)$_{0.85}$(Yttria Doped Ceria)
CHP	Combined Heat and Power
Micro-CHP	Micro-Combined Heat and Power
CCHP	Combined Cooling, Heating and Power
CHHP	Combined Heat, Hydrogen and Power
ER	Eley-Rideal
BoP	Balance of Power
AD	Anaerobic Digestion
GA	Gasification Agent
TPB	Triple Phase Boundary
Ni-YSZ	Nickel-Yttria-Stabilized Zirconia
YSZ	Yttria-Stabilized Zirconia
Ni–$MgAl_2O_4$	Nickel–Magnesium Aluminate
Ni–MgO	Nickel–Magnesium Oxide
Ni-αAl_2O_3	Nickel-αAluminum Oxide
Ni-YSZ-CeO_2	Nickel-Yttria-Stabilized Zirconia-Cerium (IV) Oxide
Ni-GDC	Nickel–Gadolinium Doped Ceria
Au–Ni/GDC	Gold–Nickel/Gadolinium Doped Ceria
Ni–ZrO_2–CeO_2	Nickel–Zirconium Dioxide-Cerium (IV) Oxide
Bio-H_2	Bio-hydrogen
Bio-CH_4	Bio-methane
Ni/CeO_2/YSZ	Nickel-Cerium(IV) Oxide-Yttria-Stabilized Zirconia
Ni/CeO_2–Al_2O_3	Nickel/Cerium(IV) Oxide-Aluminum Oxide (Ni-based composite)
Ni-ScSZ	Nickel-Scandia Stabilized Zirconia
POM	Partial Oxidation of Methane
CFD	Computational Fluid Dynamics
SC	Steam to Carbon (ratio)

PL	Power Law
PL-1	Power Law model 1
PL-2	Power Law model 2
PL-3	Power Law model 3
PL-4	Power Law model 4
LH	Langmuir-Hinshelwood
LH-1	Langmuir-Hinshelwood model 1
LH-2	Langmuir-Hinshelwood model 2
LH-HW	Langmuir–Hinshelwood–Hougen–Watson
LHV	Lower Heating Value
0D	Zero–dimensional
1D	One–dimensional
2D	Two–dimensional
FO	First-Order
Ni-CGO	Nickel-Ceria Gadolinium Oxide
Ni-SDC	Ni-Samarium Doped Ceria
Ni–ZrO_2	Nickel–Zirconium Dioxide
H–SOFCs	Steam in proton conductive SOFCs
AD	Anaerobic digestion
CaPP	Car as Power Plant
FCEVs	Fuel Cell Electric Vehicles
CR	Catalytic Reformer
SOFCR	SOFC operating as reformer
CCS	Carbon Capture and Storage
Cu/ZnO/Al_2O_3	Copper/Zinc Oxide/Aluminium Oxide
Fe_2O_3/Cr_2O_3/MgO	Ferric Oxide/Chromium Oxide/Magnesium Oxide
Ni–Al_2O_4/MgO_2	Nickel-Aluminate/Magnesium Dioxide
Ni–Al_2O_3	Nickel–Aluminum Oxide
Ni–Re	Nickel–Rhenium
Ni–CeO_2	Nickel–Cerium(IV) Oxide

Latin symbols

V	Voltage
R	Reaction rate
E_a	Activation energy
R	Ideal gas constant
T	Temperature

Subscripts

K_j	Temperature dependence of the adsorption coefficient
$K_{eq,wgs}$	Equilibrium constant for the WGS reaction
k_i	Rate coefficient
$p^a_{CH_4}$	Partial pressures of methane
$p^b_{H_2O}$	Partial pressures of steam
$p^c_{H_2}$	Partial pressures of hydrogen
p^d_{CO}	Partial pressures of carbon monoxide
a	Reaction orders of methane
b	Reaction orders of steam
c	Reaction orders of hydrogen
d	Reaction orders of carbon monoxide
p_{O_2}	Partial pressure of oxygen
p_{H_2O}	Partial pressure of steam
p_{CH_4}	Partial pressures of methane
p_{H_2}	Partial pressure of hydrogen
p_{CO}	Partial pressures of carbon monoxide
X_1	Active site 1
X_2	Active site 2
S_0	Proportional to the vacant surface
n	Number of sites involved in the molecular reaction
k_0	Rate Constant
k	Reaction Rate Pre-Exponential Factor
Q_{msr}	Quotient of the reaction

K_{msr} Equilibrium constant for the MSR reaction
K_i Equilibrium constant for adsorption
K_{eq} Equilibrium constant
y_i Concentrations of reagents in mole fraction

References

[1] Freedman M, Jaggi B. Global warming, commitment to the Kyoto protocol, and accounting disclosures by the largest global public firms from polluting industries. Int J Account 2005;40(3):215–32.
[2] Agreement P. Paris agreement. In: Report of the Conference of the Parties to the United Nations Framework Convention on Climate Change (21st Session, 2015: Paris). Retrieved December. HeinOnline; 2015.
[3] Rafiee A, et al. Biogas as an energy vector. Biomass Bioenergy 2021;144:105935.
[4] Middelhoff E, et al. Hybrid concentrated solar biomass (HCSB) plant for electricity generation in Australia: design and evaluation of techno-economic and environmental performance. Energy Convers Manag 2021;240:114244.
[5] Binder M, et al. Hydrogen from biomass gasification. IEA Bioenergy; 2018.
[6] Abanades S, et al. A critical review of biogas production and usage with legislations framework across the globe. Int J Environ Sci Technol 2022;19(4):3377–400.
[7] Hosseinnia H, Mohammadi-Ivatloo B, Mohammadpourfard M. Optimal techno-economic planning of a smart parking lot—combined heat, hydrogen, and power (SPL-CHHP)-Based microgrid in the active distribution network. Appl Sci 2021;11(17):8043.
[8] Anderson A, et al. Effects of nanofluids on the photovoltaic thermal system for hydrogen production via electrolysis process. Int J Hydrogen Energy 2022;In press.
[9] Zhou S, et al. Research on low-carbon energy transformation of China necessary to achieve the Paris agreement goals: a global perspective. Energy Econ 2021;95:105137.
[10] Thiruselvi D, et al. A critical review on global trends in biogas scenario with its up-gradation techniques for fuel cell and future perspectives. Int J Hydrogen Energy 2021;46(31):16734–50.
[11] Nandimandalam H, Gude VG, Marufuzzaman M. Environmental impact assessment of biomass supported electricity generation for sustainable rural energy systems-A case study of Grenada County, Mississippi, USA, vol. 802. Science of The Total Environment; 2022. p. 149716.
[12] Kanimozhi B, et al. Effects of oxyhydrogen on the CI engine fueled with the biodiesel blends: a performance, combustion and emission characteristics study. Int J Hydrogen Energy 2021;In press.
[13] Gunasekar P, Manigandan S, Tr PK. Hydrogen as the futuristic fuel for the aviation and aerospace industry–review. Aircraft Engineering and Aerospace Technology; 2020.
[14] Outlook IEA. For biogas and biomethane: prospects for organic growth. IEA Paris; 2020.
[15] Marcoberardino GD, et al. Green hydrogen production from raw biogas: a techno-economic investigation of conventional processes using pressure swing adsorption unit. Processes 2018;6(3):19.
[16] Chen L, et al. Catalytic hydrogen production from methane: a review on recent progress and prospect. Catalysts 2020;10(8):858.
[17] Minh DP, et al. A review on the impact of operating conditions, catalyst deactivation and regeneration in tri-reforming of methane. Applied Catalysis A: General; 2021.
[18] Minh DP, et al. Review on the catalytic tri-reforming of methane-Part I: impact of operating conditions, catalyst deactivation and regeneration. Appl Catal Gen 2021;621:118202.
[19] de Vasconcelos BR, et al. Regeneration study of Ni/hydroxyapatite spent catalyst from dry reforming. Catal Today 2018;310:107–15.
[20] Teramoto K, et al. Direct reforming of Methane–Ammonia mixed fuel on Ni–YSZ anode of solid oxide fuel cells. Int J Hydrogen Energy 2020;45(15):8965–74.
[21] Gür TM. Comprehensive review of methane conversion in solid oxide fuel cells: prospects for efficient electricity generation from natural gas. Prog Energy Combust Sci 2016;54:1–64.
[22] Ebrahimi A, et al. Biomass gasification process integration with Stirling engine, solid oxide fuel cell, and multi-effect distillation. J Therm Anal Calorim 2021;145(3):1283–302.
[23] Radenahmad N, et al. A review on biomass derived syngas for SOFC based combined heat and power application. Renew Sustain Energy Rev 2020;119:109560.
[24] Aravind PV, de Jong W. Evaluation of high temperature gas cleaning options for biomass gasification product gas for Solid Oxide Fuel Cells. Prog Energy Combust Sci 2012;38(6):737–64.
[25] Jimenez-Navarro J-P, et al. Coupling the heating and power sectors: the role of centralised combined heat and power plants and district heat in a European decarbonised power system. Appl Energy 2020;270:115134.
[26] Mahian O, et al. Exergy analysis in combined heat and power systems: a review. Energy Convers Manag 2020;226:113467.
[27] Arsalis A. A comprehensive review of fuel cell-based micro-combined-heat-and-power systems. Renew Sustain Energy Rev 2019;105:391–414.
[28] Martinez S, et al. Micro-combined heat and power systems (micro-CHP) based on renewable energy sources. Energy Convers Manag 2017;154:262–85.
[29] Sohani A, Rezapour S, Sayyaadi H. Comprehensive performance evaluation and demands' sensitivity analysis of different optimum sizing strategies for a combined cooling, heating, and power system. J Clean Prod 2021;279:123225.
[30] Mehrpooya M, et al. Technical performance analysis of a combined cooling heating and power (CCHP) system based on solid oxide fuel cell (SOFC) technology–A building application. Energy Convers Manag 2019;198:111767.
[31] Herrando M, et al. Solar combined cooling, heating and power systems based on hybrid PVT, PV or solar-thermal collectors for building applications. Renew Energy 2019;143:637–47.
[32] Chahartaghi M, Kharkeshi BA. Performance analysis of a combined cooling, heating and power system with PEM fuel cell as a prime mover. Appl Therm Eng 2018;128:805–17.
[33] Bornapour M, et al. Optimal stochastic coordinated scheduling of proton exchange membrane fuel cell-combined heat and power, wind and photovoltaic units in micro grids considering hydrogen storage. Appl Energy 2017;202:308–22.
[34] Soleymani E, Gargari SG, Ghaebi H. Thermodynamic and thermoeconomic analysis of a novel power and hydrogen cogeneration cycle based on solid SOFC. Renew Energy 2021;177:495–518.
[35] Nakashima RN, De Oliveira S. Thermodynamic evaluation of solid oxide fuel cells converting biogas into hydrogen and electricity. Int J Therm 2021;24(3):204–14.
[36] Sun C, Hui R, Roller J. Cathode materials for solid oxide fuel cells: a review. J Solid State Electrochem 2010;14(7):1125–44.
[37] Shabri HA, et al. Recent progress in metal-ceramic anode of solid oxide fuel cell for direct hydrocarbon fuel utilization: a review. Fuel Process Technol 2021;212:106626.
[38] Singh M, Zappa D, Comini E. Solid oxide fuel cell: decade of progress, future perspectives and challenges. Int J Hydrogen Energy 2021;46(54):27643–74.
[39] Sengodan S, et al. Advances in reforming and partial oxidation of hydrocarbons for hydrogen production and fuel cell applications. Renew Sustain Energy Rev 2018;82:761–80.
[40] Lyu Z, Li H, Han M. Electrochemical properties and thermal neutral state of solid oxide fuel cells with direct internal reforming of methane. Int J Hydrogen Energy 2019;44(23):12151–62.
[41] Lyu Z, Shi W, Han M. Electrochemical characteristics and carbon tolerance of solid oxide fuel cells with direct internal dry reforming of methane. Appl Energy 2018;228:556–67.
[42] Saadabadi SA, et al. Solid oxide fuel cells fuelled with biogas: potential and constraints. Renew Energy 2019;134:194–214.
[43] Hussain S, Yangping L. Review of solid oxide fuel cell materials: cathode, anode, and electrolyte. Energy Trans 2020:1–14.
[44] Fan L, et al. Methane steam reforming reaction in solid oxide fuel cells: influence of electrochemical reaction and anode thickness. J Power Sources 2021;507:230276.
[45] Fan L, et al. Study of methane steam reforming kinetics in operating solid oxide fuel cells: influence of current density. Int J Hydrogen Energy 2015;40(15):5150–9.
[46] Liu Y, Shao Z, Mori T. Development of nickel based cermet anode materials in solid oxide fuel cells–Now and future. Mater Rep: Energy 2021;1(1):100003.
[47] Tabish AN, et al. Computational fluid dynamics modeling of anode-supported solid oxide fuel cells using triple-phase boundary-based kinetics. J Power Sources 2021;513:230564.
[48] Wang J, et al. Efficient conversion of methane into power via microchanneled solid oxide fuel cells. J Power Sources 2020;453:227848.
[49] Sadykov VA, et al. Advanced materials for solid oxide fuel cells and membrane catalytic reactors. Adv Nanomater Catal Energy 2019:435–514.
[50] Chen B, et al. Combined methane reforming by carbon dioxide and steam in proton conducting solid oxide fuel cells for syngas/power co-generation. Int J Hydrogen Energy 2019;44(29):15313–21.
[51] Abdelkareem MA, et al. On the technical challenges affecting the performance of direct internal reforming biogas solid oxide fuel cells. Renew Sustain Energy Rev 2019;101:361–75.
[52] Cai L, et al. Study on the reaction pathways of steam methane reforming for H2 production. Energy 2020;207:118296.
[53] Bobrova L, et al. Water–gas shift reaction over Ni/CeO2 catalysts. Catalysts 2017;7(10):310.
[54] Abdulrasheed A, et al. A review on catalyst development for dry reforming of methane to syngas: recent advances. Renew Sustain Energy Rev 2019;108:175–93.
[55] Carapellucci R, Giordano L. Steam, dry and autothermal methane reforming for hydrogen production: a thermodynamic equilibrium analysis. J Power Sources 2020;469:228391.
[56] Saadabadi SA, Illathukandy B, Aravind PV. Direct internal methane reforming in biogas fuelled solid oxide fuel cell; the influence of operating parameters. Energy Sci Eng 2021;9(8):1232–48.
[57] Wang Y, et al. Analysis of a biogas-fed SOFC CHP system based on multi-scale hierarchical modeling. Renew Energy 2021;163:78–87.

[58] Wasajja H, et al. Techno-economic review of biogas cleaning technologies for small scale off-grid solid oxide fuel cell applications. Fuel Process Technol 2020; 197:106215.
[59] Liu J, Ryu J-H. Combined heat, hydrogen and power production from seaweed biogas-fueled solid oxide fuel cell (sofc) system. Chem Eng Trans 2020;80:163–8.
[60] Nirmal Kumar S, Appari S, Kuncharam BVR. Techniques for overcoming sulfur poisoning of catalyst employed in hydrocarbon reforming. Catal Surv Asia 2021: 1–27.
[61] Lai K-Y, Manthiram A. Self-regenerating Co–Fe nanoparticles on perovskite oxides as a hydrocarbon fuel oxidation catalyst in solid oxide fuel cells. Chem Mater 2018;30(8):2515–25.
[62] Hanna J, et al. Fundamentals of electro-and thermochemistry in the anode of solid-oxide fuel cells with hydrocarbon and syngas fuels. Prog Energy Combust Sci 2014;40:74–111.
[63] Faheem HH, et al. A review on mathematical modelling of direct internal reforming-solid oxide fuel cells. J Power Sources 2022;520:230857.
[64] Van Biert L, et al. Dynamic modelling of a direct internal reforming solid oxide fuel cell stack based on single cell experiments. Appl Energy 2019;250:976–90.
[65] Chen B, et al. Syngas/power cogeneration from proton conducting solid oxide fuel cells assisted by dry methane reforming: a thermal-electrochemical modelling study. Energy Convers Manag 2018;167:37–44.
[66] Santarelli M, et al. Direct reforming of biogas on Ni-based SOFC anodes: modelling of heterogeneous reactions and validation with experiments. J Power Sources 2013;242:405–14.
[67] Papurello D, Lanzini A. SOFC single cells fed by biogas: experimental tests with trace contaminants. Waste Manag 2018;72:306–12.
[68] Din ZU, Zainal Z. The fate of SOFC anodes under biomass producer gas contaminants. Renew Sustain Energy Rev 2017;72:1050–66.
[69] Papurello D, Canuto D, Santarelli M. CFD model for tubular SOFC stack fed directly by biomass. Int J Hydrogen Energy 2022;47(10):6860–72.
[70] Somano V, et al. CFD model for tubular SOFC directly fed by biomass. Int J Hydrogen Energy 2021;46(33):17421–34.
[71] Ahmed K, Föger K. Analysis of equilibrium and kinetic models of internal reforming on solid oxide fuel cell anodes: effect on voltage, current and temperature distribution. J Power Sources 2017;343:83–93.
[72] Yi Y, et al. Fuel flexibility study of an integrated 25 kW SOFC reformer system. J Power Sources 2005;144(1):67–76.
[73] Audasso E, Bianchi FR, Bosio B. 2D simulation for CH4 internal reforming-SOFCs: an approach to study performance degradation and optimization. Energies 2020; 13(16):4116.
[74] Xu H, et al. Modeling of all porous solid oxide fuel cells. Appl Energy 2018;219: 105–13.
[75] Van Herle J, et al. Modeling and experimental validation of solid oxide fuel cell materials and stacks. J Eur Ceram Soc 2005;25(12):2627–32.
[76] Fan L, et al. Prediction of the performance of a solid oxide fuel cell fuelled with biosyngas: influence of different steam-reforming reaction kinetic parameters. Int J Hydrogen Energy 2013;38(1):510–24.
[77] Fan L, et al. Computational studies for the evaluation of fuel flexibility in solid oxide fuel cells: a case with biosyngas. Fuel Cell 2013;13(3):410–27.
[78] van Biert L, Visser K, Aravind P. Intrinsic methane steam reforming kinetics on nickel-ceria solid oxide fuel cell anodes. J Power Sources 2019;443:227261.
[79] Thattai AT, van Biert L, Aravind PV. On direct internal methane steam reforming kinetics in operating solid oxide fuel cells with nickel-ceria anodes. J Power Sources 2017;370:71–86.
[80] Yang W, et al. First principles study on methane reforming over Ni/TiO 2 (110) surface in solid oxide fuel cells under dry and wet atmospheres. Sci China Mater 2020;63(3):364–74.
[81] Minette F, et al. Intrinsic kinetics of steam methane reforming on a thin, nanostructured and adherent Ni coating. Appl Catal B Environ 2018;238:184–97.
[82] Mogensen D, et al. Methane steam reforming over an Ni-YSZ solid oxide fuel cell anode in stack configuration. J Chem 2014;2014.
[83] Achenbach E, Riensche E. Methane/steam reforming kinetics for solid oxide fuel cells. J Power Sources 1994;52(2):283–8.
[84] Xu J, Froment GF. Methane steam reforming, methanation and water gas shift: I. Intrinsic kinetics. AIChE J 1989;35(1):88–96.
[85] Lehnert W, Meusinger J, Thom F. Modelling of gas transport phenomena in SOFC anodes. J Power Sources 2000;87(1–2):57–63.
[86] Dicks A, Pointon K, Siddle A. Intrinsic reaction kinetics of methane steam reforming on a nickel/zirconia anode. J Power Sources 2000;86(1–2):523–30.
[87] Hou K, Hughes R. The kinetics of methane steam reforming over a Ni-alpha-Al2O catalyst. Chem Eng J 2001;82(1–3):311–28.
[88] Brus G, et al. An experimental and theoretical approach for the carbon deposition problem during steam reforming of model biogas. J Theor Appl Mech 2015;53.
[89] Timmermann H, et al. Internal reforming of methane at Ni/YSZ and Ni/CGO SOFC cermet anodes. Fuel Cell 2006;6(34):307–13.
[90] Mogensen D. Methane steam reforming kinetics over Ni-YSZ anode materials for Solid Oxide Fuel Cells. 2011.
[91] Ahmed K, Foger K. Kinetics of internal steam reforming of methane on Ni/YSZ-based anodes for solid oxide fuel cells. Catal Today 2000;63(2–4):479–87.
[92] Bebelis S, et al. Intrinsic kinetics of the internal steam reforming of CH4 over a Ni-YSZ-cermet catalyst-electrode. Ind Eng Chem Res 2000;39(12):4920–7.
[93] Zhu H, et al. Modeling elementary heterogeneous chemistry and electrochemistry in solid-oxide fuel cells. J Electrochem Soc 2005;152(12):A2427.
[94] Sciazko A, et al. A novel approach to the experimental study on methane/steam reforming kinetics using the Orthogonal Least Squares method. J Power Sources 2014;262:245–54.
[95] King DL, et al. Effect of nickel microstructure on methane steam-reforming activity of Ni–YSZ cermet anode catalyst. J Catal 2008;258(2):356–65.
[96] Wei J, Iglesia E. Isotopic and kinetic assessment of the mechanism of reactions of CH4 with CO2 or H2O to form synthesis gas and carbon on nickel catalysts. J Catal 2004;224(2):370–83.
[97] Helfferich FG. Kinetics of multistep reactions. Elsevier; 2004.
[98] Hecht ES, et al. Methane reforming kinetics within a Ni–YSZ SOFC anode support. Appl Catal Gen 2005;295(1):40–51.
[99] Janardhanan VM, Deutschmann O. CFD analysis of a solid oxide fuel cell with internal reforming: coupled interactions of transport, heterogeneous catalysis and electrochemical processes. J Power Sources 2006;162(2):1192–202.
[100] Jones G, et al. First principles calculations and experimental insight into methane steam reforming over transition metal catalysts. J Catal 2008;259(1):147–60.
[101] Arcotumapathy V, et al. Mechanistic investigation of methane steam reforming over Ce-promoted Ni/SBA-15 catalyst. Appl Petrochem Res 2015;5(4):393–404.
[102] Hofmann P, et al. Operation of solid oxide fuel cell on biomass product gas with tar. Int J Hydrogen Energy 2009;34(22):9203–12.
[103] Delgado KH, et al. Surface reaction kinetics of steam-and CO2-reforming as well as oxidation of methane over nickel-based catalysts. Catalysts 2015;5(2): 871–904.
[104] Yadavalli SS, Jones G, Stamatakis M. DFT benchmark studies on representative species and poisons of methane steam reforming on Ni (111). Phys Chem Chem Phys 2021;23(29):15601–12.
[105] Niu J, et al. New mechanism insights into methane steam reforming on Pt/Ni from DFT and experimental kinetic study. Fuel 2020;266:117143.
[106] Wang B, et al. Propagating DFT uncertainty to mechanism determination, degree of rate control, and coverage analysis: the kinetics of dry reforming of methane. J Phys Chem C 2019;123(50):30389–97.
[107] Che F, et al. Improving Ni catalysts using electric fields: a DFT and experimental study of the methane steam reforming reaction. ACS Catal 2017;7(1):551–62.
[108] Mendes D, et al. The water-gas shift reaction: from conventional catalytic systems to Pd-based membrane reactors-a review. Asia Pac J Chem Eng 2010;5(1): 111–37.
[109] Elnashaie SSEH, et al. On the non-monotonic behaviour of methane-steam reforming kinetics. Chem Eng Sci 1990;45(2):491–501.
[110] Klein J-M, et al. Direct methane solid oxide fuel cell working by gradual internal steam reforming: analysis of operation. J Power Sources 2009;193(1):331–7.
[111] Wang Y, et al. Performance and effective kinetic models of methane steam reforming over Ni/YSZ anode of planar SOFC. Int J Hydrogen Energy 2009;34(9): 3885–93.
[112] Belyaev V, et al. Internal steam reforming of methane over Ni-based electrode in solid oxide fuel cells. Appl Catal Gen 1995;133(1):47–57.
[113] Nakagawa N, Sagara H, Kato K. Catalytic activity of Ni–YSZ–CeO2 anode for the steam reforming of methane in a direct internal-reforming solid oxide fuel cell. J Power Sources 2001;92(1–2):88–94.
[114] Riensche E, et al. Clean combined-cycle SOFC power plant–cell modelling and process analysis. J Power Sources 2000;86(1–2):404–10.
[115] Parsons J, Randall S. Experimental determination of kinetic rate data for SOFC anodes. SOFC-Micromodelling IEA-SOFC-Task Report; 1992. p. 43–6.
[116] Lee AL, Zabransky R, Huber W. Internal reforming development for solid oxide fuel cells. Ind Eng Chem Res 1990;29(5):766–73.
[117] Souentie S, et al. Mathematical modeling of Ni/GDC and Au–Ni/GDC SOFC anodes performance under internal methane steam reforming conditions. J Catal 2013;306:116–28.
[118] Grzegorz B, et al. An analysis of biogas reforming process on Ni/YSZ and Ni/SDC catalysts. Int J Therm 2012;15(1):43–51.
[119] Belyaev V, Politova T, Sobyanin V. Effect of non-Faradaic electrochemical modification of catalytic activity. Solid State Ionics 2000;136:721–5.
[120] Amran UI, Ahmad A, Othman MR. Kinetic based simulation of methane steam reforming and water gas shift for hydrogen production using aspen plus. Chem Eng Trans 2017;56:1681–6.
[121] Chen B, et al. Modelling of one-step methanation process combining SOECs and Fischer-Tropsch-like reactor. J Electrochem Soc 2016;163(11):F3001.
[122] Choi Y, Stenger HG. Water gas shift reaction kinetics and reactor modeling for fuel cell grade hydrogen. J Power Sources 2003;124(2):432–9.
[123] Rj BS, Loganathan M, Shantha MS. A review of the water gas shift reaction kinetics. Int J Chem React Eng 2010;8(1).
[124] Wheeler C, et al. The water–gas-shift reaction at short contact times. J Catal 2004; 223(1):191–9.
[125] Krupay BW, Ross RA. The kinetics of the water–gas shift reaction on nickel (II) oxide catalysts in the néel temperature region. Can J Chem 1974;52(17):3063–9.
[126] Wolf A, Jess A, Kern C. Syngas production via reverse water-gas shift reaction over a Ni-Al2O3 catalyst: catalyst stability, reaction kinetics, and modeling. Chem Eng Technol 2016;39(6):1040–8.
[127] Dong X, et al. Intrinsic kinetics study of biogas methanation coupling with water gas shift over Re-promoted Ni bifunctional catalysts. Catalysts 2019;9(5):422.
[128] Rafique M, et al. Material and method selection for efficient solid oxide fuel cell anode: recent advancements and reviews. Int J Energy Res 2019;43(7):2423–46.
[129] Aramouni NAK, et al. Catalyst design for dry reforming of methane: analysis review. Renew Sustain Energy Rev 2018;82:2570–85.
[130] Shaikh SP, Muchtar A, Somalu MR. A review on the selection of anode materials for solid-oxide fuel cells. Renew Sustain Energy Rev 2015;51:1–8.
[131] Gorte R, Vohs J. Catalysis in solid oxide fuel cells. Ann Rev Chem Biomol Eng 2011;2:9–30.
[132] Atkinson A, et al. Advanced anodes for high-temperature fuel cells. Mater Sustain Energy: Collect Peer-Rev Res Rev Artic Nat Publ Group 2011:213–23.

[133] Zhu W, Deevi S. A review on the status of anode materials for solid oxide fuel cells. Mater Sci Eng, A 2003;362(1–2):228–39.
[134] Tao S, Irvine JT. Discovery and characterization of novel oxide anodes for solid oxide fuel cells. Chem Rec 2004;4(2):83–95.
[135] Fu Q, Tietz F. Ceramic-based anode materials for improved redox cycling of solid oxide fuel cells. Fuel Cell 2008;8(5):283–93.
[136] Dicks A. Advances in catalysts for internal reforming in high temperature fuel cells. J Power Sources 1998;71(1–2):111–22.
[137] Meusinger J, Riensche E, Stimming U. Reforming of natural gas in solid oxide fuel cell systems. J Power Sources 1998;71(1–2):315–20.
[138] Eguchi K, et al. Fuel flexibility in power generation by solid oxide fuel cells. Solid State Ionics 2002;152:411–6.
[139] Eguchi K, et al. Electrical properties of ceria-based oxides and their application to solid oxide fuel cells. Solid State Ionics 1992;52(1–3):165–72.
[140] Zhu H, et al. A new nickel-ceria composite for direct-methane solid oxide fuel cells. Int J Hydrogen Energy 2013;38(9):3741–9.
[141] Mogensen M, Skaarup S. Kinetic and geometric aspects of solid oxide fuel cell electrodes. Solid State Ionics 1996;86:1151–60.
[142] Park S, Vohs JM, Gorte RJ. Direct oxidation of hydrocarbons in a solid-oxide fuel cell. Nature 2000;404(6775):265–7.
[143] Park S, et al. Direct oxidation of hydrocarbons in a solid oxide fuel cell: I. Methane oxidation. J Electrochem Soc 1999;146(10):3603.
[144] Putna E, et al. Ceria-based anodes for the direct oxidation of methane in solid oxide fuel cells. Langmuir 1995;11(12):4832–7.
[145] Murray EP, Tsai T, Barnett SA. A direct-methane fuel cell with a ceria-based anode. Nature 1999;400(6745):649–51.
[146] Lanzini A, Leone P. Experimental investigation of direct internal reforming of biogas in solid oxide fuel cells. Int J Hydrogen Energy 2010;35(6):2463–76.
[147] Farhad S, Hamdullahpur F, Yoo Y. Performance evaluation of different configurations of biogas-fuelled SOFC micro-CHP systems for residential applications. Int J Hydrogen Energy 2010;35(8):3758–68.
[148] Gunji A, et al. Carbon deposition behaviour on Ni-ScSZ anodes for internal reforming solid oxide fuel cells. J Power Sources 2004;131(1):285–8.
[149] Fan D, et al. Autothermal reforming of methane over an integrated solid oxide fuel cell reactor for power and syngas co-generation. J Power Sources 2021;513:230536.
[150] Tu B, et al. High performance of direct methane-fuelled solid oxide fuel cell with samarium modified nickel-based anode. Int J Hydrogen Energy 2020;45(51):27587–96.
[151] Fan D, et al. A microchannel reactor-integrated ceramic fuel cell with dual-coupling effect for efficient power and syngas co-generation from methane. Appl Catal B Environ 2021:120443.
[152] Panagi K, et al. Highly efficient coproduction of electrical power and synthesis gas from biohythane using solid oxide fuel cell technology. Appl Energy 2019;255:113854.
[153] Fernandes A, et al. Fuel cell electric vehicle as a power plant and SOFC as a natural gas reformer: an exergy analysis of different system designs. Appl Energy 2016;173:13–28.
[154] Mozdzierz M, et al. An afterburner-powered methane/steam reformer for a solid oxide fuel cells application. Heat Mass Tran 2018;54(8):2331–41.
[155] Gorte RJ, et al. Anodes for direct oxidation of dry hydrocarbons in a solid-oxide fuel cell. Adv Mater 2000;12(19):1465–9.
[156] Li L, et al. Hydrogen production via steam reforming of n-dodecane over NiPt alloy catalysts. Fuel 2020;262:116469.
[157] Wang H, Zhao H, Zhao Z. Thermodynamic performance study of a new SOFC–CCHP system with diesel reforming by CLHG to produce hydrogen as fuel. Int J Hydrogen Energy 2021;46(44):22956–73.
[158] Mehrpooya M, Ghorbani B, Abedi H. Biodiesel production integrated with glycerol steam reforming process, solid oxide fuel cell (SOFC) power plant, vol. 206. Energy Conversion and Management; 2020. p. 112467.
[159] Ashok J, et al. Steam reforming of surrogate diesel model over hydrotalcite-derived MO-CaO-Al2O3 (M= Ni & Co) catalysts for SOFC applications. Fuel 2021;291:120194.
[160] Leone P, et al. Methane-free biogas for direct feeding of solid oxide fuel cells. J Power Sources 2010;195(1):239–48.
[161] Minutillo M, Perna A, Sorce A. Combined hydrogen, heat and electricity generation via biogas reforming: energy and economic assessments. Int J Hydrogen Energy 2019;44(43):23880–98.
[162] Ou Z, et al. Highly active and stable Ni/perovskite catalysts in steam methane reforming for hydrogen production. Sustain Energy Fuels 2021;5(6):1845–56.
[163] Dawood F, Anda M, Shafiullah G. Hydrogen production for energy: an overview. Int J Hydrogen Energy 2020;45(7):3847–69.
[164] Setiabudi H, et al. Hydrogen production from catalytic steam reforming of biomass pyrolysis oil or bio-oil derivatives: a review. Int J Hydrogen Energy 2020;45(36):18376–97.
[165] Bian Z, et al. A review on perovskite catalysts for reforming of methane to hydrogen production. Renew Sustain Energy Rev 2020;134:110291.
[166] Acar C, Dincer I. Review and evaluation of hydrogen production options for better environment. J Clean Prod 2019;218:835–49.
[167] Kannah RY, et al. Techno-economic assessment of various hydrogen production methods–A review. Bioresour Technol 2021;319:124175.
[168] Abdalla AM, et al. Hydrogen production, storage, transportation and key challenges with applications: a review. Energy Convers Manag 2018;165:602–27.
[169] Weiland P. Biogas production: current state and perspectives. Appl Microbiol Biotechnol 2010;85(4):849–60.
[170] Ivers-Tiffée E, Weber A, Herbstritt D. Materials and technologies for SOFC-components. J Eur Ceram Soc 2001;21(10–11):1805–11.
[171] Choi H, Cho GY, Cha S-W. Fabrication and characterization of anode supported YSZ/GDC bilayer electrolyte SOFC using dry press process. Int J Precis Eng Manuf -Green Technol 2014;1(2):95–9.
[172] Faes A, Hessler-Wyser A, Zryd A. A review of RedOx cycling of solid oxide fuel cells anode. Membranes 2012;2(3):585–664.
[173] He L, et al. A new perspective of co-doping and Nd segregation effect on proton stability and transportation in Y and Nd co-doped BaCeO3. Int J Hydrogen Energy 2021;46(1):1096–105.
[174] Lee W, et al. Cation size mismatch and charge interactions drive dopant segregation at the surfaces of manganite perovskites. J Am Chem Soc 2013;135(21):7909–25.
[175] Huber A-K, et al. In situ study of electrochemical activation and surface segregation of the SOFC electrode material La 0.75 Sr 0.25 Cr 0.5 Mn 0.5 O 3±δ. Phys Chem Chem Phys 2012;14(2):751–8.
[176] Hodjati-Pugh O, Dhir A, Steinberger-Wilckens R. Internal current collection and thermofluidynamic enhancement in a microtubular SOFC. Int J Heat Mass Tran 2021;173:121255.
[177] Zhu H, Kee RJ. The influence of current collection on the performance of tubular anode-supported SOFC cells. J Power Sources 2007;169(2):315–26.
[178] Wu J, Liu X. Recent development of SOFC metallic interconnect. J Mater Sci Technol 2010;26(4):293–305.
[179] Zhu WZ, Deevi SC. Development of interconnect materials for solid oxide fuel cells. Mater Sci Eng 2003;348(1–2):227–43.
[180] Yang Z, et al. Selection and evaluation of heat-resistant alloys for SOFC interconnect applications. J Electrochem Soc 2003;150(9):A1188.
[181] Huang B, Qi Y, Murshed M. Solid oxide fuel cell: perspective of dynamic modeling and control. J Process Control 2011;21(10):1426–37.
[182] Aguiar P, Adjiman CS, Brandon NP. Anode-supported intermediate-temperature direct internal reforming solid oxide fuel cell: II. Model-based dynamic performance and control. J Power Sources 2005;147(1):136–47.
[183] Li YH, Choi SS, Rajakaruna S. An analysis of the control and operation of a solid oxide fuel-cell power plant in an isolated system. Energy Conv IEEE Trans 2005;20(2):381–7.
[184] Shi N, et al. Review of anodic reactions in hydrocarbon fueled solid oxide fuel cells and strategies to improve anode performance and stability. Mater Renew Sustain Energy 2020;9(1):1–18.
[185] Badwal S, et al. Review of progress in high temperature solid oxide fuel cells. ChemInform 2015;46(31) [p. no-no].
[186] Badwal S. Stability of solid oxide fuel cell components. Solid State Ionics 2001;143(1):39–46.
[187] Cowin PI, et al. Recent progress in the development of anode materials for solid oxide fuel cells. Adv Energy Mater 2011;1(3):314–32.
[188] Kim G, et al. Investigation of the structural and catalytic requirements for high-performance SOFC anodes formed by infiltration of LSCM. Electrochem Solid State Lett 2009;12(3):B48.
[189] Vohs JM, Gorte RJ. High-performance SOFC cathodes prepared by infiltration. Adv Mater 2009;21(9):943–56.
[190] Li Y, et al. Composition and toxicity of biogas produced from different feedstocks in California. Environ Sci Technol 2019;53(19):11569–79.
[191] Kamalimeera N, Kirubakaran V. Prospects and restraints in biogas fed SOFC for rural energization: a critical review in Indian perspective. Renew Sustain Energy Rev 2021;143:110914.
[192] Gao Y, et al. A review of recent developments in hydrogen production via biogas dry reforming. Energy Convers Manag 2018;171:133–55.
[193] Boldrin P, et al. Strategies for carbon and sulfur tolerant solid oxide fuel cell materials, incorporating lessons from heterogeneous catalysis. Chem Rev 2016;116(22):13633–84.
[194] Hong J, et al. Sulfur poisoning and performance recovery of SOFC air electrodes. Front Energy Res 2021;9.
[195] Katariya H, Patolia H. Advances in biogas cleaning, enrichment, and utilization technologies: a way forward. Biomass Conversion and Biorefinery; 2021. p. 1–17.